NUCLEAR FUEL CYCLES

BEHAVIOR OF MODERN METALLIC FUEL IN TREAT TRANSIENT OVERPOWER TESTS

THEODORE H. BAUER, ARTHUR E. WRIGHT, WILLIAM R. ROBINSON, JOHN W. HOLLAND, and EDGAR A. RHODES *Argonne National Laboratory Reactor Analysis and Safety Division, 9700 South Cass Avenue Argonne, Illinois 60439*

Received November 9, 1989
Accepted for Publication March 5, 1990

Results and analyses of margin to cladding failure and prefailure axial expansion of metallic fuel are reported for Transient Reactor Test Facility in-pile transient overpower tests M2 through M7. These include the first such tests on binary and ternary alloy fuel of the Integral Fast Reactor concept and fuel burnups to 10 at.%. The fuel was tested at full coolant flow and subjected to an exponential power rise on an 8-s period until either incipient or actual cladding failure was achieved. Objectives, designs, and methods are described with emphasis on developments unique to metal fuel safety testing. Test results include the following: (a) temperature, flow, and pressure data; (b) fuel motion diagnostic data from the fast neutron hodoscope; and (c) test remains described by both destructive and nondestructive posttest examination. The resulting M-series data base for cladding failure threshold and prefailure fuel expansion is presented. The nature of the observed cladding failure and resultant fuel dispersals is described. Simple models of cladding failures and prefailure axial expansions are presented and compared with experimental results.

I. INTRODUCTION

Acceptable safety-related behavior and performance of modern metal fuel is a key element in the development of the Integral Fast Reactor (IFR) concept, an innovative liquid-metal reactor (LMR) design.[1] For the IFR concept to be successful, it is necessary that metal fuel itself demonstrate a high level of inherent or passive safety that extends well beyond normal operating conditions.

To help meet this need, a series of experiments was performed at the Transient Reactor Test Facility (TREAT) between 1984 and 1987. The aim of these experiments (designated tests M2 through M7) was the study of cladding failure threshold and other safety-related fuel behavior during simulated transient overpower (TOP) accidents.

The data needs specifically addressed by these tests are as follows:

1. determination of margin to failure and identification of underlying mechanisms
2. assessment of prefailure axial expansion as a potentially significant prefailure reactivity removal mechanism
3. preliminary assessment of postfailure events, i.e., behavior of disrupted fuel and coolant.

Overpower testing in the TREAT reactor draws on >20 yr experience in transient safety testing in flowing sodium loops and allows for controlled transient overheating of whole fuel pins by fission in a near-prototypic thermal and hydraulic environment. For the IFR experiments, preirradiated fuel was tested. Each test pin in this series was subjected to similar overpower conditions in a simulated TOP accident, i.e., full coolant flow and an exponential power rise on an 8-s period. Attention was centered on the time domain of cladding failure threshold. Particular requirements included stopping the power transient on the brink of failure for some pins and just after failure for others. To meet programmatic needs, it was important to test many pins quickly, despite the limited availability of test hardware and of TREAT reactor time. Thus, the concept of testing two (or more) pins simultaneously, with separate and possibly different hydraulic environments for each pin, was actively pursued.

II. THE TEST FUEL

Many of the positive safety-related aspects of metallic fuel performance during both normal and off-normal conditions follow from design attributes common to all modern metal fuel types.[1,2] These include (a) efficient heat transfer to coolant through high-conductivity fuel and a sodium bond between fuel and cladding, and (b) a high tolerance for fuel swelling and efficient release of fission gas to the pin plenum. The M-series tests extended existing fuel performance studies into far off-normal TOP conditions. It was important to test many fuel and cladding combinations relevant to the IFR concept with a wide a range of fuel burnups in order to distinguish features of fuel-specific safety-related fuel performance from those that are common to all modern metal fuel types.

The source of the irradiated fuel tested in M-series is the Experimental Breeder Reactor II (EBR-II), the metal-fueled fast reactor prototype operated by Argonne National Laboratory (ANL). Due to early availability of irradiated fuel and because it had been well-characterized, initial tests (M2, M3, and M4) in the series used EBR-II driver fuel made of a binary alloy of uranium and fissium (U-Fs). (Fissium is a mixture of metals representing an equilibrium composition of fission products after reprocessing.) Later tests (M5, M6, and M7) used IFR-type fuel that had been preirradiated in EBR-II, as appropriate test pins became available. Reference fuel for the IFR concept uses uranium, plutonium, and zirconium in ternary (U-Pu-Zr) and binary (U-Zr) compositions. Nominal design dimensions of all M-series test pins are listed in Table I.

In all cases, the preirradiation in EBR-II was intended to mimic the temperatures and restructuring of full-length (~1-m-long) fuel. The EBR-II fuel pin environment includes a 34-cm active core height, an average-to-peak axial power ratio of 0.92, and a coolant temperature rise of ~100 K commencing from a nominal 644 K value at the inlet. Irradiation power levels for the IFR-type pins in EBR-II were ~36 to 40 kW/m axial peak. This power level is significantly higher than the ~25 kW/m axial peak power in the irradiation of the U-Fs fuel. In comparison, a 40 kW/m peak power level, 630 K inlet temperature, and 150 K coolant temperature rise are assumed to be nominal values for an IFR-type fast reactor throughout this paper.

A considerable amount of restructuring takes place during irradiation of all modern metal fuel, which influences both fuel morphology and thermal properties.[2-4] During the first several atom percent of burnup, the fuel swells by as much as 50% of its original size until it makes contact with the cladding. The liquid sodium bond originally surrounding the fuel slug is displaced into the pin's gas plenum. Much of the fuel volume increase is comprised of gas-filled pores, but interconnection of pores leads to both release of fission gas to the plenum and infiltration of the porosity network by liquid bond sodium. Pressure in the plenum is influenced principally by fission gas release from fuel. After swelled fuel contacts the cladding, there is little further swelling and total fuel volume remains approximately constant with increasing burnup. However, further burnup leads to the accumulation of solid and liquid fission products at a rate of ~1 vol%/at.% of burnup, which tends to further reduce pore volumes filled with gas.

Such fuel restructuring is directly relevant to the issues studied in the M-series tests. Fuel swelling, infiltration of porosity by sodium, and accumulation of solid and liquid fission products strongly influence fuel thermal conductivity and onset of fuel melting. Gas retention within the fuel supplies a potential driving mechanism for prefailure elongation, whereas gas release from the fuel adds to an internal pin pressure that drives cladding failure. If the temperature is sustained at abnormally high levels, close contact between fuel and cladding can lead to the formation of low-temperature molten phases that can damage and eventually penetrate the cladding.

Restructuring also differs somewhat among various metal fuel types. Sample fuel cross sections from irradiated pins similar to some of those tested in M-series are shown in Fig. 1. In IFR ternary fuel, a three-zone radial structure develops that includes multiple irregularities, separations, and cracks. Irregularities in fuel-cladding gap closure are also noted at low burnup. These zones represent a migration of both zirconium and porosity toward the outside and some buildup of

TABLE I

Nominal Design Parameters of M-Series Test Pins

	U-Fs	IFR-Type
Fuel		
Length (mm)	343	343
Diameter of slug (mm)	3.30	4.32
Mass (g)	52	78
Radial smear density (%) (to cladding inner diameter)	75	72.5
Bond sodium		
Initial height above fuel (mm)	~28	6.35
Total volume (cm^3)	~1.3	2.0
Gas plenum		
Length above sodium (mm)	193	246
Volume (initial) (cm^3)	2.2	5.0
Cladding		
Outside diameter (mm)	4.42	5.84
Inside diameter (mm)	3.81	5.08
Thickness (mm)	0.30	0.38

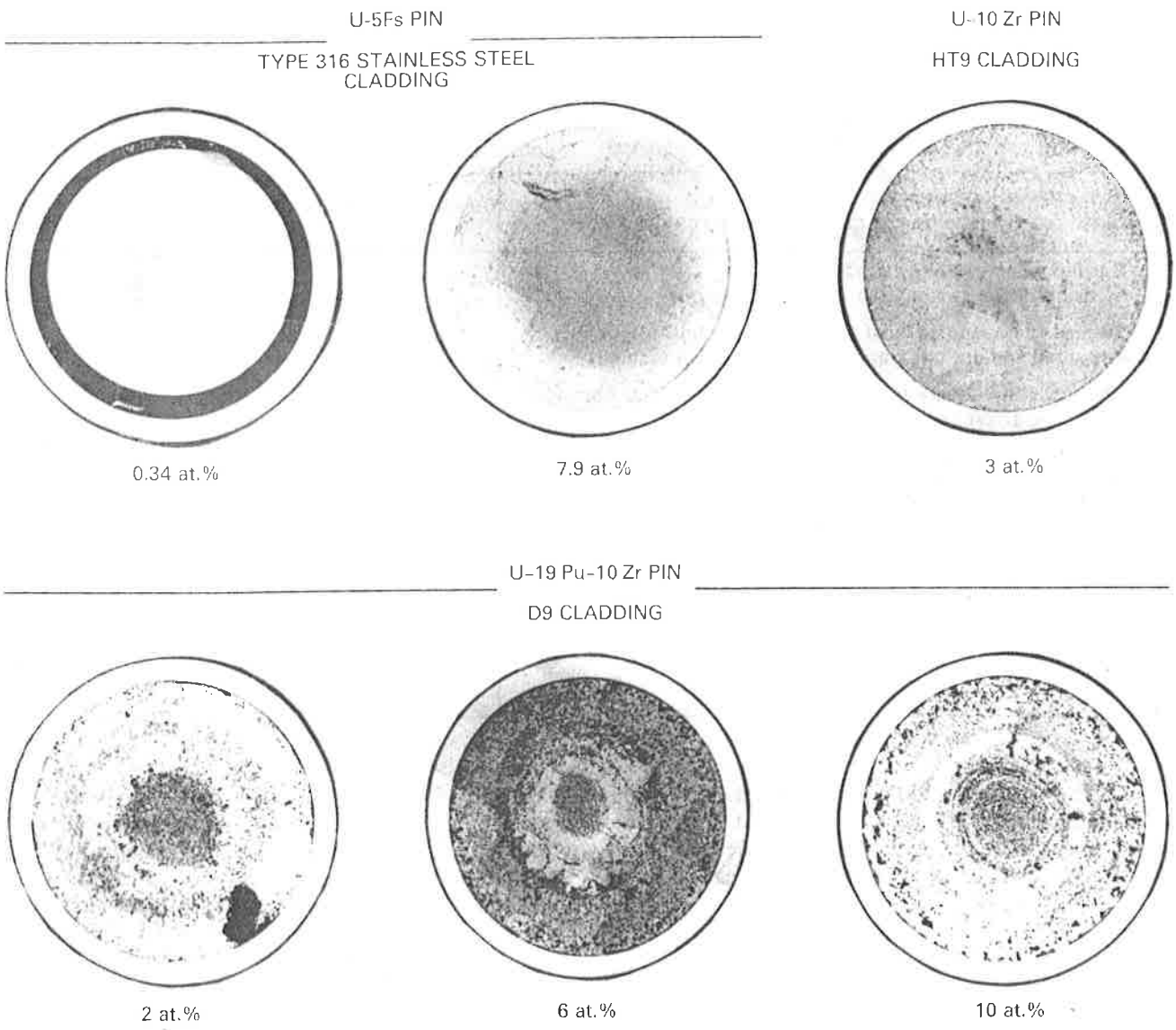

Fig. 1. Representative midplane cross sections of untested siblings to M-series test fuel.

heavy metal concentration midradius. Both IFR binary and U-Fs fuels restructure more uniformly.

Fission gas release from metallic fuel seems to depend strongly on fuel temperature during irradiation,[5] emphasizing the importance of irradiation power level and fuel thermal conductivity. (Gas residing within large fuel pores is considered to be released from the fuel matrix.) Due to their higher irradiation power level, IFR-type test fuel typically retained a much smaller concentration of gas in the fuel matrix than did U-Fs test fuel.

Table II lists compositions and summarizes average characteristics of irradiated M-series test fuel based on measurements of fuel swelling, sodium logging within porosity, and plenum pressurization.[2-4] The effect of restructuring on thermal conductivity can be large. The burnup dependence of thermal conductivity shown in Table II was calculated by a model that estimates effects of both gas-filled and sodium-logged porosity and is normalized to agree with available measurements on U-Fs fuel.[6-8]

III. FACILITIES AND TEST HARDWARE

III.A. Major Facilities

The TREAT reactor, located at the ANL-West site within the Idaho National Engineering Laboratory, is a uranium- and graphite-fueled reactor with a near-thermal neutron spectrum. A cutaway view is shown in

TABLE II

Approximate Pretest Characteristics of Irradiated M-Series Fuel

	Fuel Alloy (composition wt%)		
	U-19 Pu-10 Zr	U-10 Zr	U-5 Fs
Peak irradiation power level (kW/m)	38	38	25
Measured gas retention as generated in the indicated burnup (at.%)	~0.5	~0.5	2
Burnup when swelling saturates (at.%)	1	1	2
Measured axial swelling (% of original height)	2 to 3	8 to 9	4 to 5
Swelled fuel volume (% of total fuel volume)	29	32	28
Measured sodium infiltration (% of total fuel volume)	8	13	6
Thermal conductivity at 1000 K (W/cm·K) average burnup			
0 at.% (fresh)	0.23	0.34	0.40
2 at.%	~0.15	~0.21	~0.20
10 at.%	~0.20	~0.30	~0.33
Melting point (K)			
Solidus	1350	1508	1283
Liquidus	1515	1678	1373
Measured gas plenum pressure at room temperature at the indicated peak burnup (MPa)			
0 at.% (fresh)	0.10	0.10	0.10
5 at.%	2.3	2.3	2.5
10 at.%	5.1	5.1	6.0

Fig. 2. Fast-operating computer-operated control rods provide the capability of a wide range of power transients appropriate for reactor safety studies. A forced-air cooling system provides a limited heat rejection capability at low power levels. However, in the high-power transient mode most commonly used for safety testing, the reactor heats up nearly adiabatically. While adiabatic core heating contributes significantly to safe operation, it also results in limits to transient energy deposition due to both maximum allowable core temperatures and large negative reactivity feedback. In the M-series tests, transient energy deposition in the test fuel was limited to the equivalent of several tens of seconds of full-power operation.

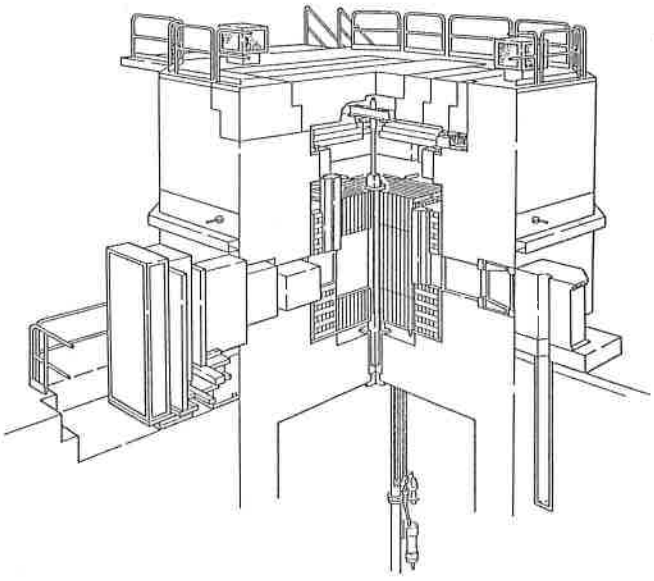

Fig. 2. TREAT reactor cutaway showing test vehicle at the centerline. The fast neutron hodoscope slot and detectors are shown to the left.

Most experiments performed in TREAT require the use of the fast neutron hodoscope,[9] also shown in Fig. 2. The TREAT hodoscope is a diagnostic system that looks through a slot in the TREAT core to collimate and detect fast neutrons produced by fissions in the test fuel. Analysis of this data results in a test fuel motion history in two dimensions with data collection at submillisecond to millisecond time intervals. Fast neutrons from the test fuel can generally be distinguished from the dominant background of thermal neutrons from TREAT by their energy. In M-series, the hodoscope was used in conjunction with a full-slotted core (core slots both in front of and behind the test loop hardware). Such a configuration reduces the maximum energy deposition but minimizes background and provides the highest possible accuracy in fuel motion detection.

Many test support operations involving highly radioactive irradiated fuel pins and their posttest remains

need to be performed in a hot-cell environment. The Hot Fuel Examination Facility (HFEF) at ANL-West provided in-cell facilities to assemble and disassemble experiments on irradiated fuel. Nondestructive radiography and profilometry of test fuel were also performed both pre- and posttest at HFEF. Destructive examination of M-series remains, including both failed and unfailed pins, was undertaken at the Alpha Gamma Hot Cell Facility at ANL-East (Illinois).

III.B. M-Series Test Hardware

The sodium loop used in TREAT for ANL's LMR safety experiments in recent years has been the Mark-III vehicle.[10] Figure 3 shows the Mark-III loop as configured for the M-series tests. It is an elongated loop of thick-walled stainless steel pipe through which liquid sodium is circulated by an electromagnetic pump. Two parallel legs of the loop are 3.5 m long

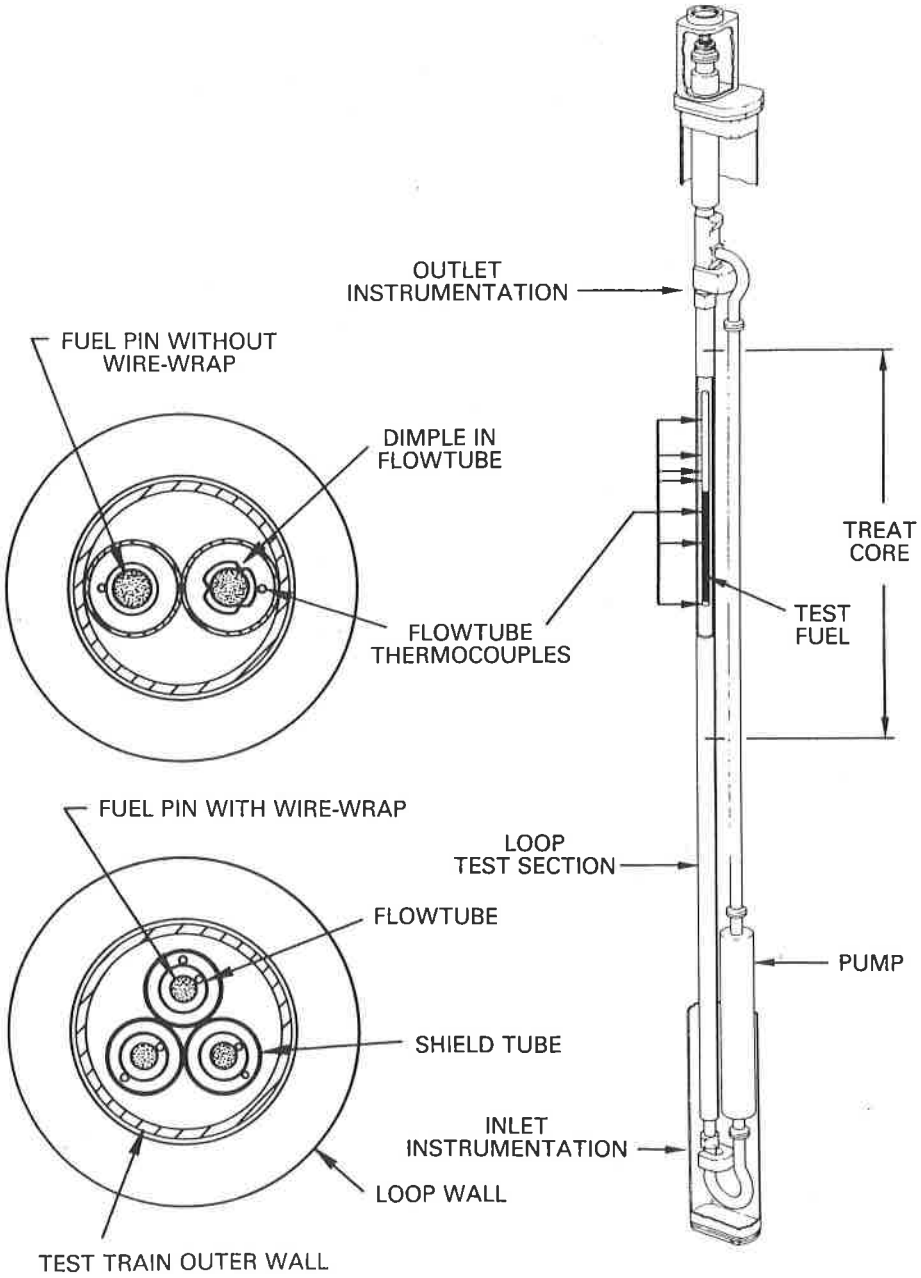

Fig. 3. Mark-III integral sodium loop as configured for M-series testing of two or three pins at one time.

with center-to-center separation of ~0.1 m. The entire system is housed in a long rectangular container of 10- × 20-cm cross-section dimensions designed to occupy the space of two TREAT fuel assemblies at the center of the reactor (see Fig. 2). The Mark-III vehicle is intended to have generic utility in testing a wide variety of test fuel types and bundles. A removable test train in one leg of the loop contains an instrumented test fuel configuration that is designed to meet specific program requirements. This test leg also includes an extension that serves as a gas plenum and provides the entrance through which the test train is inserted into the loop. The other leg of the loop includes a small annular linear induction pump to drive the sodium coolant. In operation, sodium flows upward past the test fuel. Thermal-hydraulic conditions in the loop are measured by three permanent-magnet flowmeters, two pressure transducers, and numerous thermocouples.

In the specific test trains used in the M-series, each pin was located in a separate stainless steel flowtube, with the division of total loop sodium flow into the flowtubes chosen to achieve the particular objectives for each pin. This division was achieved by properly sized orifices installed near the entrance to each flowtube. The lateral separation of test pins was as wide as possible to minimize the neutron shielding of one pin by another and to enhance the ability of the hodoscope to resolve test pins as individual entities. The number of pins per test was determined principally by the bore diameter of the Mark-III sodium loop. As shown in Fig. 3, three small-diameter U-Fs fuel pins were included in tests M2, M3, and M4; two IFR-type pins were included in tests M5, M6, and M7.

Coolant temperatures at the outlet and along the fuel zone were measured using thermocouples intrinsically attached to the outer surface of each flowtube. The flowtubes were made as thin as possible (<0.5 mm) so that the test fuel and the flowtube-mounted thermocouples would be as closely thermally coupled as possible. The flowtubes were isolated from each other and the rest of the test hardware by a shield tube placed around each flowtube with low-conductivity inert gas in between. The shield tube prevents large amounts of debris released from one failed flowtube from damaging an adjacent flowtube. So far, these protective features of the shield tubes were not needed in the four M-series tests performed where fuel pins failed. Flowtube breach occurred in only a single instance and was scarcely detectable.

The ability to reuse expensive and slow-to-build test hardware contributed to the timely performance of the test program. All six M-series experiments were performed in only two test loops. Test trains were reused following the two experiments where the test fuel did not fail. However, because debris from failed fuel remained largely confined to the removable test train, loops could be reused even after pin failures. Hardware performance demonstrated a high degree of reliability; however, some problems did occur in hydraulically seating test trains in loops that had been used several times. These problems were attributed to debris accumulation in the loop sodium, but all seating difficulties were resolved in advance of experiment performance.

Although the principal instrument of nuclear diagnostics at TREAT is the fast neutron hodoscope, attempts were also made to detect release and transport of fission products from failed fuel. During later tests, fission products from failed fuel that were transported to the loop cover gas region were measured by a developmental fission product detection system (FPDS). A horizontal collimator passes through the concrete reactor biological shield and selects a region of the loop 1.5 m above the center of the core. Depending on the vertical placement of the loop, the FPDS can observe either the uppermost part of the sodium or the gas space above it. Detectors are situated outside the concrete shield. Presently, the ability to detect radioactive fission products and delayed neutrons is very limited and, because of an unfavorable signal-to-background ratio, no measurements can be made until after the TREAT power transient is over.

III.C. Hardware Development During M-Series

During the test program, a number of design improvements were made to better adapt test train hardware to experiment needs and to observed behavior of metal fuel.

In the area of test fuel support, early tests (M2, M3, and M4) used wire-wrapped pins directly in smooth flowtubes. Metal fuel pins are mechanically weak at high temperature, and a single wire-wrapped pin in a smooth flowtube provides poor support against distortion. It was believed that this method of support permitted pin bowing and flexing that caused both hard-to-explain temperature oscillations at high temperature, and hard-to-analyze irregularities or periodicities in the measured axial temperature rise at all temperatures. To alleviate these problems in M5, M6, and M7, test pin wire-wraps, which had provided spacing and support during the EBR-II preirradiation, were removed. Pin support was provided instead by dimples in the flowtube spaced at ~10-cm axial and 120-deg azimuthal increments. While this new mounting scheme did not provide a coolant flow and contact pattern prototypical of a wire-wrapped pin in a large bundle, it was intended to provide the test fuel with a commensurate level of resistance to warping and distortion. Improvements resulting from this new mounting scheme were noted, but some irregularities and high-temperature oscillations remained in M5 and M6 data. These remaining problems were attributed to the fuel pins not being sufficiently centered. Consequently, in M7 the axial spacing between supporting dimples was decreased while the dimple depth was increased to provide the greatest possible centering consistent with

a minimal clearance needed to insert test pins within the tube. These modifications significantly reduced observed temperature anomalies in M7. Figure 4 shows the effect of the improved pin-support methods on temperature measurements made along the test pin flowtube.

Attention was also given to reducing uncertainties in the measurement of coolant flow past each test pin. The combined sodium flow rate during a test is measured by calibrated permanent-magnet flowmeters at the inlet and outlet of the test section as well as in the pump leg of the loop. In the initial M-series tests, flow division among test pins was inferred on the basis of symmetry and separate hydraulic measurements performed out-of-pile. However, beginning with M5, two miniature permanent-magnet flowmeters were also located near the inlet of each individual flowtube. Although the absolute sensitivities of these flowmeters were not determined, both were identical in design and layout so that the ratio of their output signals was used to determine the ratio of flow rates in the two tubes.

IV. TEST DESIGN AND TECHNIQUES

IV.A. General Features

The design of all M-series tests had a number of general features in common. Low-power, nondestructive operation verified equipment performance as well as the neutronic coupling of the test fuel to the TREAT reactor. The subsequent overpower transient was designed to generate thermal conditions in test fuel that mimic fuel overheated under fast reactor conditions. Finally, the overpower transient was terminated quickly enough to preserve conditions that existed at the peak of the overpower. Preliminary discussions of M-series test design and techniques have already been reported.[11,12]

Heat balance transients, run at constant power and flow rate, were performed before each overpower transient to provide an integrated check of the thermal-hydraulic operation of the entire experiment system including the reactor, test fuel, and sodium loop. However, a key measurement made during the heat balance was a coolant temperature rise from inlet to outlet under true steady-state conditions. This temperature rise provided a direct, *in situ* measurement of each test pin's *P/F* ratio of test fuel power *P* to coolant flow rate *F*, bypassing uncertainties in the reactor to test fuel power coupling, division of flow between flowtubes, etc.

For example, Fig. 5 shows the power history, total coolant flow rate, and temperature rise past a ternary fuel pin measured at different axial elevations during an M7 heat balance. The results are typical of heat balances performed in the test series. The various thermocouples attached to the flowtube above the active fuel height ($X/L > 1$) agree closely and can be used to determine a whole-pin temperature rise midway through the power transient. In this example, the temperature rise achieved was ~141 K (or a *P/F* ratio of 0.94 times an assumed nominal value of 150 K) at a reactor power of ~46 MW and at a total coolant flow rate of ~162 cm^3/s.

In the analysis of M-series overpower transients, the *P/F* ratio is the most important single parameter that can be used as a measure of the severity of test conditions. The key phenomena controlling safety issues (see Sec. VI) are either driven by or are closely correlated with peak coolant temperature, and the thermal response of a fuel pin is sufficiently fast that coolant temperatures are very close to steady-state values determined by *P/F*. Unfortunately, rapidly changing temperatures during overpower transients preclude direct measurements of *P/F*, as described above for heat balances.

However, because the operating conditions of the heat balance and ensuing overpower transient were in many respects identical, a straightforward proportioning technique was used to extrapolate *P/F* measurements made in a heat balance to *P/F* levels achieved during the subsequent overpower transient. Specifically, the overpower *P/F* was obtained by multiplying the measured *P/F* in the heat balance by the appropriate ratio of measured reactor power (final to heat balance) and the appropriate ratio of measured flow rate (heat balance to final).

All peak overpower levels reported here were obtained in this manner. Based on the consistency of measured temperature rises, the accuracy of these determinations is believed to be ~5% in the earlier tests (M2, M3, and M4), improving somewhat in later tests (M5, M6, and M7). This same technique also enabled the peak *P/F* values obtained in each overpower transient to be fine-tuned just before the test by appropriate adjustments of the applied flow rate or reactor power transient. Finally, once the coolant flow rate past a test pin is determined, the *P/F* measurement in the heat balance also determines the pin-average power coupling of the reactor to the test fuel (see Sec. IV.B).

In performing the final overpower transients, all test fuel in this series was subjected to similar overpower conditions: full coolant flow and an exponential power rise on an 8-s period. The 8-s period was chosen as the slowest transient possible that would commence from near-nominal power and carry through to cladding failure within the energy deposition limitations of the TREAT reactor. A high system pressure $\gtrsim$4 atm prevented coolant boiling prior to cladding failure. Baseline thermal conditions in the test fuel were referenced to conditions assumed to be nominal in a fast reactor. These include a peak linear power rating of 40 kW/m (12 kW/ft), an inlet temperature of 630 K, and a 150 K coolant temperature rise. The power transient was rapidly terminated on detection of cladding breach or, by using previously measured failure thresholds, just prior to failure.

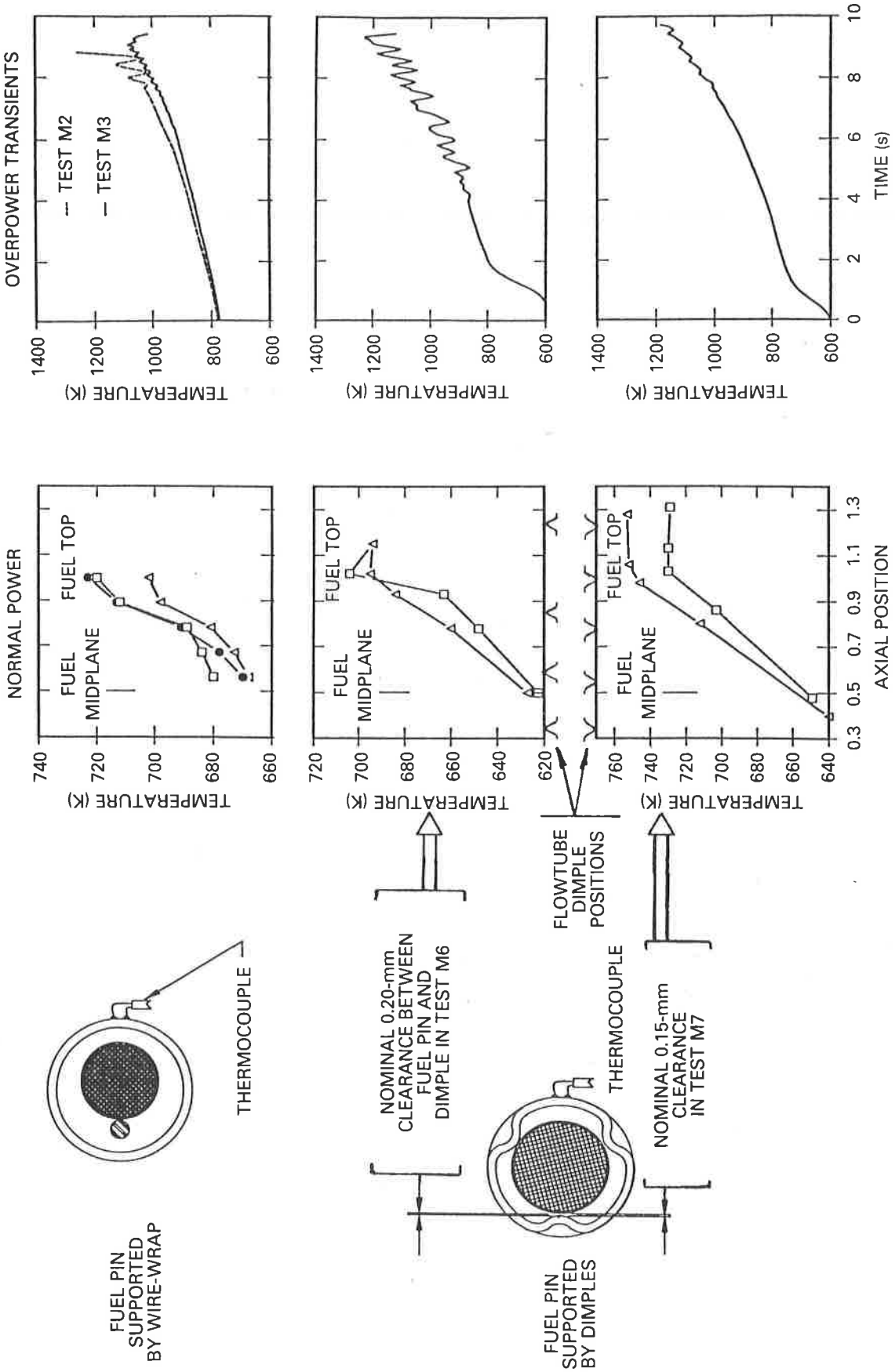

Fig. 4. Relationship of measured temperature rises and method of fuel pin support.

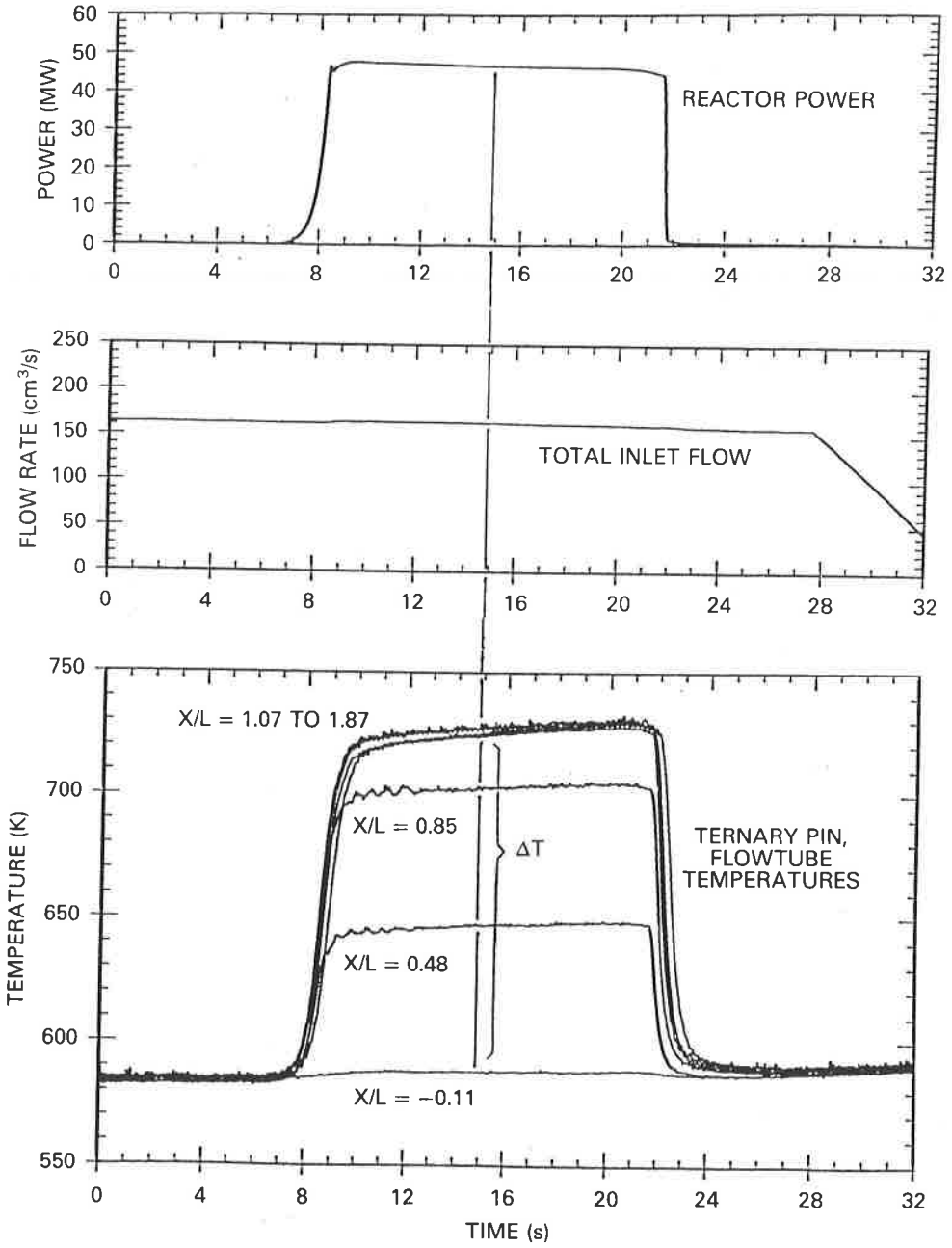

Fig. 5. Data obtained during performance of a typical M-series heat balance (M7) used to determine test pin *P/F* ratio and power coupling.

In terminating the final overpower transient, quenching the fuel at incipient failure or immediately after failure was important to preserve the state of the fuel at that instant for posttest examination. Due to the high conductivity of the metal fuel, such quenching occurred essentially on reactor power shutdown.

Sudden measurable changes in coolant flow provide the fastest and most reliable indicators of pin failures. Therefore, a system was designed in which a sudden and substantial decrease in the total sodium flow rate measured at the inlet (characteristic of coolant channel pressurization on pin failure) induced an electronic device called the shutdown signal generator to output a signal that triggered reactor shutdown. Figure 6 illustrates how the shutdown system worked using data from test M6 as an example. Note that the system was sufficiently sensitive to detect failure in only one flowtube. The shutdown signal was sent within ~10 ms of pin failure, and the reactor power began to decrease less than ~50 ms later.

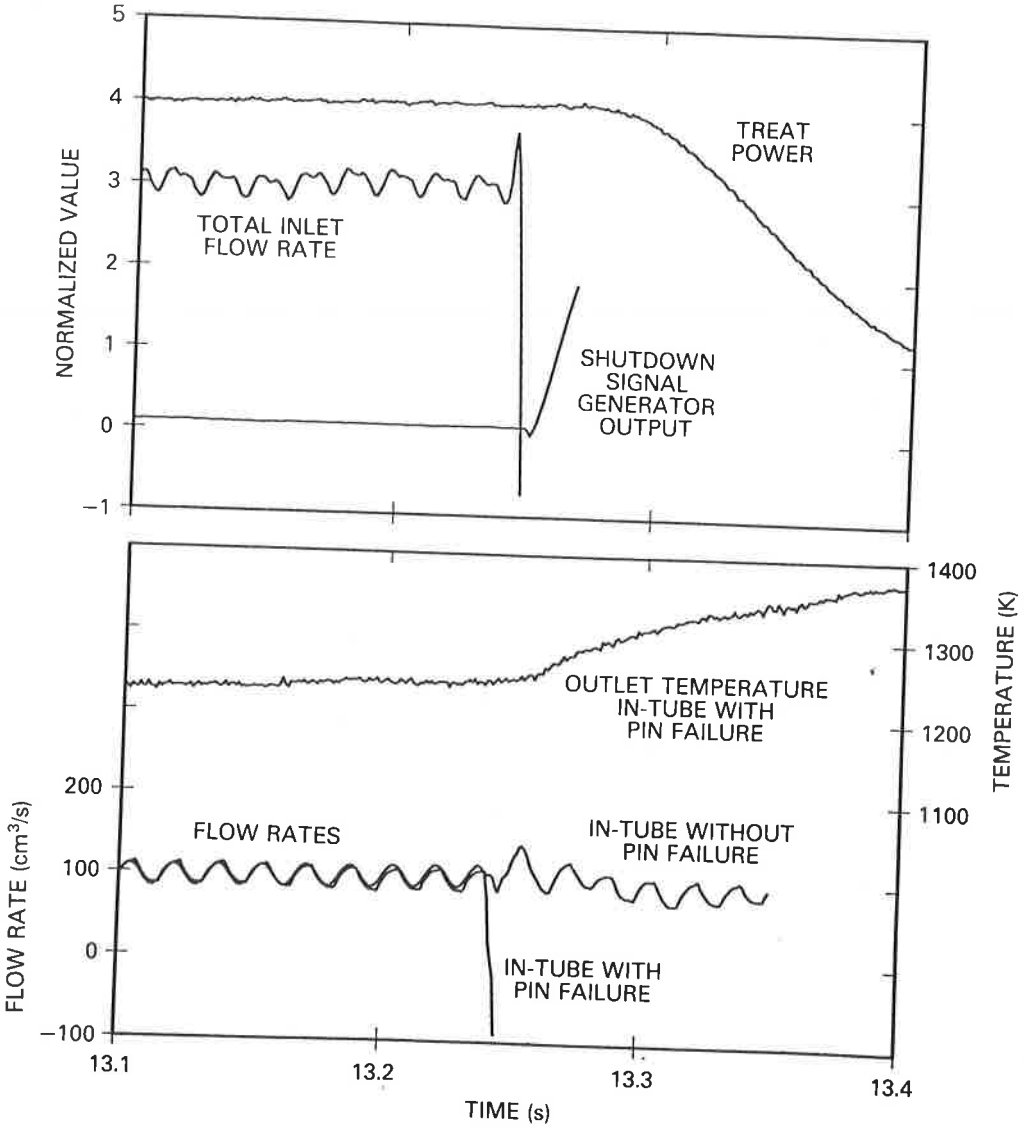

Fig. 6. Operation of the shutdown signal generator during M6.

IV.B. Power Coupling of the Test Fuel to the Reactor

Before the test conditions of any experiment can be set or any posttest analysis can take place, an accurate determination must be made of the coupling of power generated within the test fuel to the power generated by the TREAT reactor. Determinations must be made on a whole-pin basis as well as radial and axial distributions within a fuel pin. A complicating aspect of M-series testing was the significant variation of power coupling among the various test pins due to differences in initial fissile content, wide ranges of test pin burnup, and significant morphological changes in the fuel with that burnup. A variety of techniques, both experimental and analytical, employing considerable redundancy and cross checking were used to determine the power couplings in the M-series. Fundamental estimates made use of specially performed calibration experiments with fresh fuel and flux monitor wires to measure an axially dependent power coupling to fresh fuel. These were supplemented by analyses to estimate the radial distributions and the neutronic effects of burnup and swelling. Independently, an *in situ* technique, based on the coolant temperature rise measured during a heat balance, determined pin-average power coupling by multiplying measured *P/F* ratio (see Sec. IV.A) by the known coolant flow rate and dividing by known reactor power.

Statistical errors in the various fundamental calibration measurements total ~4 to 5% in estimating a

pin-average power coupling. However, calculated effects of burnup and restructuring on power coupling can be large (of order 5 to 15%) and of opposite signs. The accuracy of such calculations depends on the accuracy of the irradiated pin characterization. Systematic errors are potentially large and difficult to estimate. Based on estimates of the precision of the various elements needed in its calculation, the precision of the *in situ* determination of pin-average power coupling is similar to that obtained from fundamental estimates, ~5%, but there is less potential for serious systematic error. Agreement between heat balance and fundamental pin-average power coupling estimates was generally good. (Exceptions arose where knowledge of pin restructuring was questionable.)

Thus, for purposes of subsequent analysis, both the pin-average power coupling and primary measurements of test pin *P/F* were taken from temperature rise measurements made during the heat balances. All other features of power coupling, such as in-pin power distributions, were taken from fundamental measurements and calculations.

IV.C. Enhancement of Power and Flow Rate

Strong radial self-shielding of the TREAT thermal neutron flux by the test fuel causes a disproportionate fraction of power to be generated near the fuel surface with a surface-to-center ratio calculated to be ~3 to 1. In contrast, power generation in a fast reactor is spatially uniform over a radial cross section of a fuel pin. To generate radial temperature gradients during M-series TREAT transients that are prototypical of those that would be generated in a fast reactor, it is necessary to increase the net power generation of the TREAT test relative to that of the fast reactor reference. Under the quasi-steady-state conditions that characterize these transients, the TREAT power increase is an enhancement factor that depends on the details of the radial power dependence and test fuel thermal conductivity. For M-series test fuel, this enhancement factor ranges from ~1.25 to 1.40. However, it is also important to maintain a prototypical coolant temperature rise at any axial location, so the coolant flow rate should be increased by precisely the same enhancement factor. Thus, a prototypical power-to-flow ratio is maintained. Finally, the additional heat (~25 to 40%) generated within the test fuel in TREAT causes a corresponding increase in the temperature gradient across the cladding. This temperature increase was compensated by a decrease in coolant inlet temperature (~30 to 50 K).

In a transient simulation where power rises steadily, it was merely necessary to appropriately lower coolant inlet temperature and increase the coolant flow rate from fast reactor reference values by the appropriate enhancement factor. The benefits achieved by this technique result in significant improvement in the prototypicality of computed fuel and cladding temperature of the M-series tests. Figure 7 shows that with test condition enhancements, calculations of peak test fuel melting (which are typical of all M-series tests) show close correspondence to a fast reactor prototype case. Without enhancement, such correspondence is only approximate. As described in Sec. V.A, later M-series tests imposed enhanced rather than nominal prototypical conditions.

IV.D. Analysis Methods

Most of the phenomena under study in M-series are either directly driven or strongly influenced by transient thermal conditions produced in the tests. The small number of thermocouples on flowtube walls and at the ends of the test section necessitated significant analysis to fill in details of fuel, cladding, and coolant temperatures. Thus, a primary aim of test analysis is to obtain as accurate a thermal history of each test as possible on the basis of input power and coolant flow.

Emphasis is also placed on providing reasonable baseline estimates of thermal conditions achieved near the cladding failure threshold. Results of these calculations then provide primary thermal input for fuel performance analyses of prefailure fuel expansion, cladding damage, and failure.

The thermal-hydraulic analyses reported here used the COBRA-PI code.[13] Historically, COBRA-PI has been used extensively in analysis of TREAT in-pile experiments because of its ability to explicitly model pin bundle geometry in small-scale experiments. In this context its use has been limited, however, to intact (fixed) geometry and single-phase coolant flow. For M-series, the analysis incorporates detailed description of the fuel pin, flowing coolant, and flowtube.

The COBRA-PI fuel pin model contains multiple radial and axial nodes. Azimuthal uniformity is assumed in the present M-series model. All thermal properties are temperature dependent with a melting transition computed in the fuel on the basis of input solidus and liquidus temperatures. Fuel properties, including melting temperatures, may also be input with radial dependence. Because of the fuel's sodium bonding, fuel and cladding are assumed to be in good thermal contact. The computed fuel/cladding interface temperature is used as a basis for assessing the formation of the low melting point eutectic (see Sec. VI.B). Formation of this low-temperature molten phase under accident conditions at high temperatures is not reflected in this primary thermal analysis, but it is treated in a separate auxiliary calculation.

Axially, the M-series analysis extends the full length of a fuel pin, including both fuel and gas plenum regions with multiple axial nodes. The coolant channel geometry is axially uniform, assumes a pin centered in the flowtube, and models single radial nodes of turbulent flow thermally connected to both

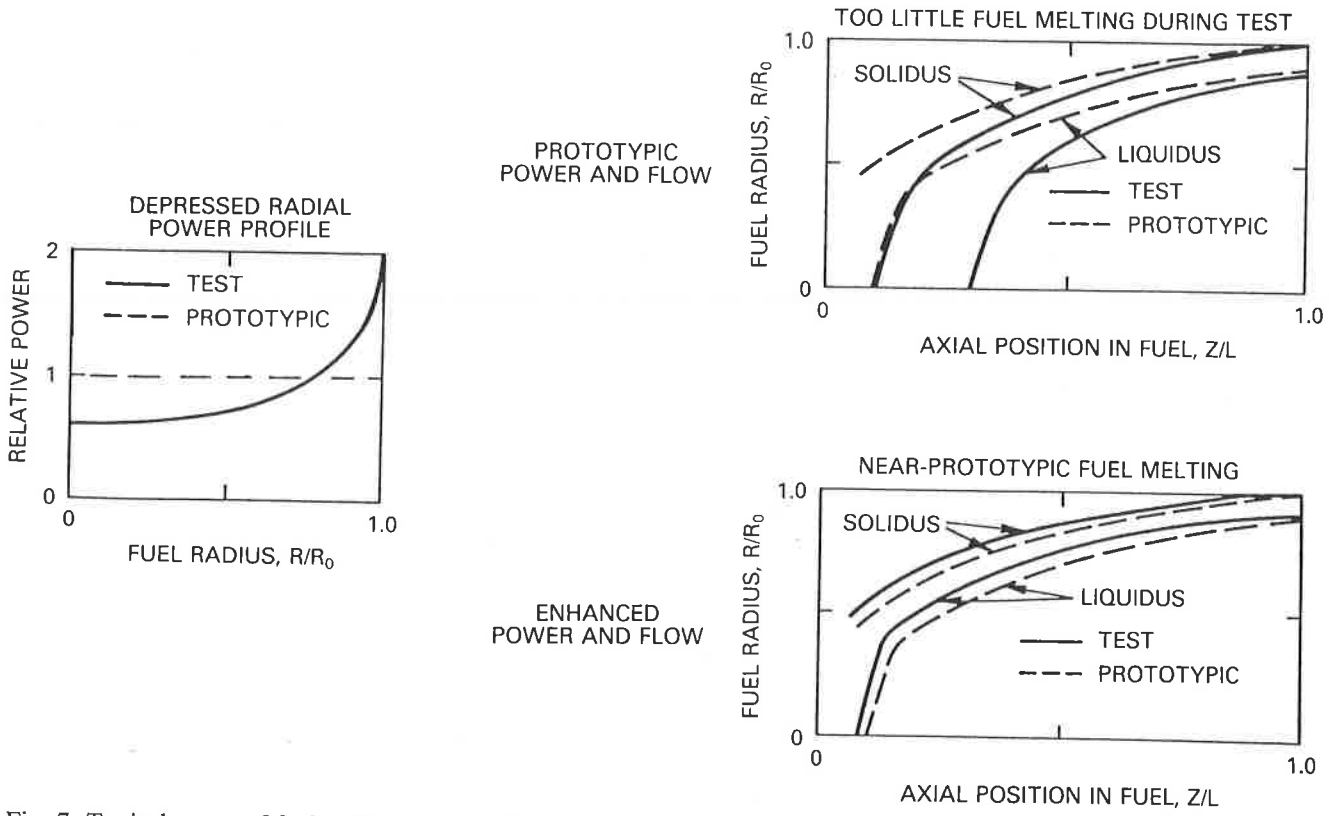

Fig. 7. Typical extent of fuel melting computed in a TREAT experiment with and without enhancement compared to a fast reactor prototype.

the pin cladding and a well-insulated flowtube. The wire-wraps or dimples used to support the pin within the flowtube are not modeled.

The fuel performance calculations of prefailure axial expansion and cladding failure were performed by a specially written routine, the Extrusion and Penetration (EXP) model that is auxiliary to the COBRA-PI code. Development and application of the EXP routine was based on modeling concepts described in Sec. VI. Logical flow of the analysis is such that transient temperatures calculated by COBRA-PI provide the driving input for the EXP, but the EXP calculations do not influence COBRA-PI. The combined program for metal fuel performance analysis is termed COBRA/EXP.

V. PERFORMANCE OF THE OVERPOWER TRANSIENTS

V.A. Test Performance and Event Sequence

Brief preliminary descriptions of individual M-series tests and their results have already been reported.[14-18] Table III summarizes overpower testing of metal fuel in the TREAT M-series to date. Nineteen pins were tested, five to beyond cladding failure. In four of the tests (M2, M4, M6, and M7), the power transient was terminated by experimental indications of a test pin failure. In the M3 failure, thresholds determined previously in M2 were used to achieve overpower conditions that came just short of failure in all three test pins. The first test of IFR-type fuel, M5 was performed under the unusually stringent practical requirement that the test train hardware be reusable after the test. Since M5 was the first test of a new fuel type, the power transient was terminated at a conservatively low preset power level to avoid pin failure. Initial results from this overpower transient indicated that the test fuel had not melted extensively nor been brought near the failure threshold. The fuel was subsequently subjected to a second power transient with a coolant flow rate reduced by 22%.

The initial tests in the program, M2 and M3, were performed at flow rate and inlet coolant temperatures near nominal for a fast reactor. Beginning with M4, test conditions were enhanced (flow rate increased and inlet temperature lowered) to provide a better match of test fuel temperature to temperature generated in a fast reactor (see Sec. IV.C). (Because it was performed with a reduced flow rate, the second overpower transient performed in M5 was the only instance among the latter tests without enhanced conditions.)

Using M7 as an example, Figs. 8 and 9 illustrate

TABLE III

Overpower Testing of Metal Fuel in TREAT M-Series

Test	Fuel (composition wt%)	Cladding	Burnup (at.%)	Date
M2	U-5 Fs	Type 316 stainless steel	0.3	March 1985
	U-5 Fs	Type 316 stainless steel	4.4	
	U-5 Fs	Type 316 stainless steel	7.9	
M3	U-5 Fs	Type 316 stainless steel	0.3	April 1985
	U-5 Fs	Type 316 stainless steel	4.4	
	U-5 Fs	Type 316 stainless steel	7.9	
M4	U-5 Fs	Type 316 stainless steel	0.0	January 1986
	U-5 Fs	Type 316 stainless steel	2.4	
	U-5 Fs	Type 316 stainless steel	7.9	
M5	U-19 Pu-10 Zr	D9	0.8	August 1986
	U-19 Pu-10 Zr	D9	1.9	
M6	U-19 Pu-10 Zr	D9	1.9	February 1987
	U-19 Pu-10 Zr	D9	5.3	
M7	U-19 Pu-10 Zr	D9	9.8	October 1987
	U-10 Zr	HT9	2.9	

typical overpower test performance and event sequence when a pin failed. Figure 8 shows the axial peak power densities applied to both test fuel pins, the resulting temperature transient measured on the outside of both flowtubes, and the flow perturbation generated by the failure of one of the test pins. The efficient heat transfer in metal fuel systems causes flowtube temperatures to closely follow applied fission power with time delays of <1 s. Prior to failure, measured flowtube temperatures closely followed adjacent coolant temperatures, and the indicated peak values on Fig. 8 (~1100 to 1200 K) were typical of these experiments and correspond closely to peak values of coolant temperatures. A sudden jump in flowtube temperature (to values indicative of coolant boiling at loop pressures of ~4 atm) coincident with the sudden reversal of inlet coolant flow marked the cladding failure of the ternary pin. The subsequent rapid power shutdown was prearranged and was triggered by the detection of sudden inlet flow reversal (as described in Sec. IV.A). The smooth response of the intact pin's flowtube temperature verifies that one pin's failure has a minimal influence on the other. Also coincident (but not shown in Fig. 8) are spikes in loop pressure transducer readings.

The transient hodographs shown in Fig. 9 describe the above sequence of events from the viewpoint of fuel motion measured by the fast neutron hodoscope. Measured fuel density, averaged over the indicated time intervals, is displayed on the two-dimensional grid. (The scale is greatly expanded horizontally. Actual pixel dimensions are ~6 mm horizontal × 34 mm vertical.) Note that the resolution is sufficient to easily distinguish the fuel columns of both M7 test pins. On Fig. 9, prefailure axial expansion is seen in both test pins as an increase of fuel density near the top and above the fuel column to hodographs a through d. The eventual failure of the ternary pin is seen dramatically in hodographs d through g by sudden fuel gains extending to great distances above the original fuel column (with corresponding losses from the remainder of the pin). The timing of this event is in good agreement with the test instrumentation, shown in Fig. 8.

V.B. Computed and Measured Heating

Comprehensive thermal-hydraulic analyses of all overpower experiments were performed with the COBRA-PI code as described in Sec. IV.D. Reactor power, measured flow rates, and measured inlet temperature were input to the computation. All computations assumed intact geometry and are useful only before cladding failure. The analyses accounted for different pin-to-reactor power coupling, thermal conductivities, and melting points of different fuel types. Nonuniform radial distributions of fuel constituents based on measurements were included for ternary fuel but did not have a large effect on computed results.

V.B.1. Flowtube and Coolant Temperature Rise

Due to the high thermal conductivity of metal fuel and the relative slowness of the power transient, calculations indicate that the time dependence of the coolant temperature rise is very sensitive to the transient

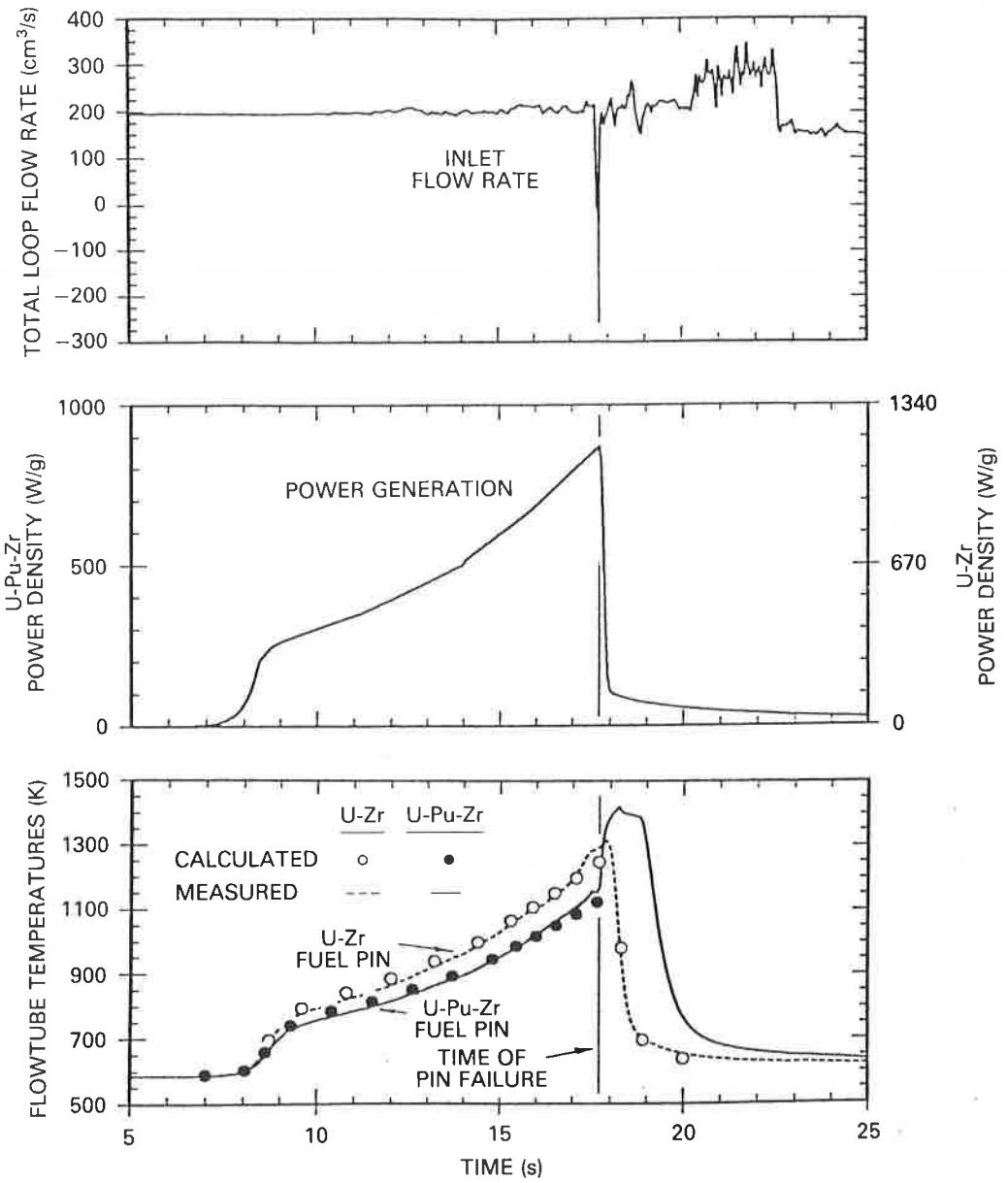

Fig. 8. Selected test results from M7 test instrumentation illustrating a typical event sequence associated with fuel pin failure.

power generation within the test fuel. Also, since the flowtube is thin and surrounded by insulating low-conductivity gas, the coolant temperature closely matches the temperature measured on the outside of the adjacent flowtube. Good agreement between the measured and computed temperature rise along the test pin flowtubes thus provides a measure of validation of the thermal-hydraulic analysis and thermal time response of the system as a whole.

Figure 8 shows such a comparison for thermocouple locations above the fuel in M7. This good agreement is typical in M-series when comparing a computed whole-pin temperature rise with the thermocouples located axially above the fuel. By design, thermocouples at these higher locations allow a maximum of time for the heat released by the test pin to be distributed radially and azimuthally within the coolant, thereby providing the most significant comparison with calculations.

V.B.2. Fuel Melting

All M-series overpower transients caused extensive melting in the test fuel amounting to approximately one-half the fuel inventory at peak power (even without considering the possibility of low-temperature molten

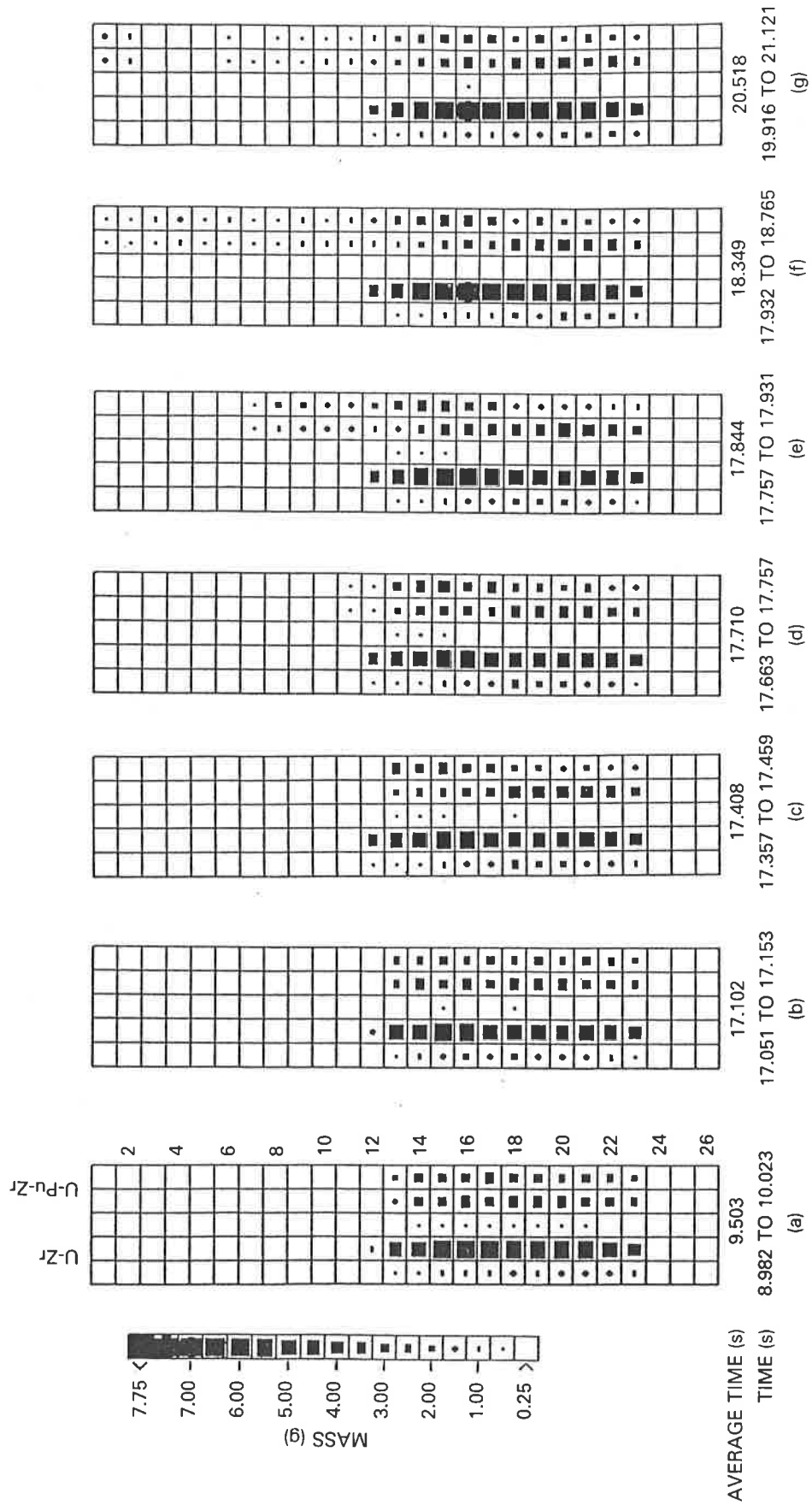

Fig. 9. Transient fuel motion observed in M7 by the fast neutron hodoscope.

phases at the fuel/cladding interface; see Sec. VI). The same thermal analyses that computed flowtube and coolant temperatures also computed fuel melting and temperature fields deep within the fuel pin. These internal temperatures were not accessible to direct measurement. However, experimental estimates of the maximum extent of melting were made during posttest microexamination of cross sections from test pins that did not fail. Agreement between these measurements and the calculations was generally good. The computed presence and amount of molten fuel provide key input to models describing prefailure axial expansion and cladding failure, and reasonable agreement of calculated maximum extent of melting with measurements validates their use in evaluating fuel performance concepts and models.

As a typical example, Fig. 10 shows computed melt profiles at peak power for M7 test pins. Measured solidus radii are included for the pin that remained intact. Note that the calculated solidus radii are quite sensitive to the input values of thermal conductivity and the many changes brought about by restructuring (see Table II). The agreement between measured and calculated solidus radii is quite reasonable.

V.C. Peak Overpower Conditions and Fuel Performance Summary

A comprehensive summary of key overpower test results is given in Table IV. Peak overpower levels and summary indicators of fuel performance are reported. In every case, some axial expansion of the test fuel was observed before failure with the peak values shown in the table. However, at low burnup, IFR-type fuel showed considerably less expansion than U-Fs fuel. Test pins were usually subjected to overpower conditions exceeding 4 times nominal. Pin failure was not observed to occur significantly below this overpower level. Calculations with a model designed to predict cladding failure indicated that those pins that remained intact were nevertheless brought quite close to failure. The calculated values of peak pin pressures are also indicated. All failure sites were located at the fuel top.

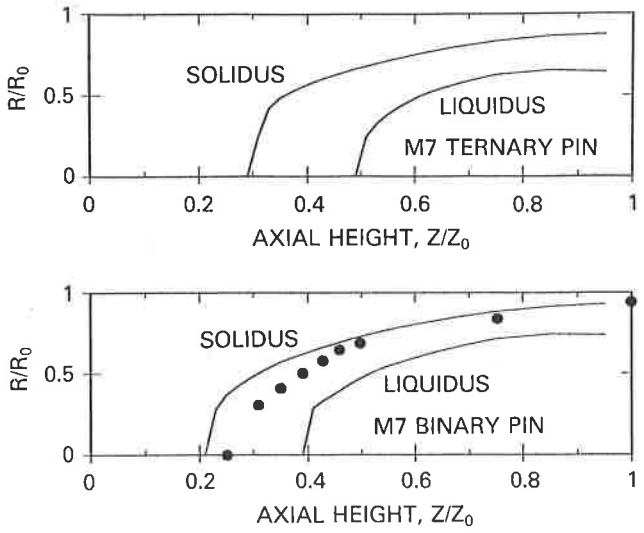

Fig. 10. Calculated maximum extent of fuel melting in M7 compared to posttest measurements made at selected axial locations in the intact pin as indicated by the dots.

As outlined in Sec. IV.A, the reported overpower levels are the peak values of the *P/F* ratio obtained directly by extrapolation from the steady-state coolant temperature rises measured in heat balances, and they carry an uncertainty of 3 to 5%. Reported overpower levels signify peak thermal conditions (temperatures, amount of melting, pressures, etc.) appropriate to a fast reactor. As discussed in Secs. IV.C and V.A, this correspondence is better in later tests where test conditions were enhanced relative to nominal.

Details of observed fuel performance are discussed in Sec. VI, which emphasizes the underlying phenomena, mechanisms, and ingredients needed for computational models. In particular, mechanisms and models of cladding failure threshold and prefailure fuel expansion are proposed, described, and critically evaluated. Some preliminary versions of these M-series fuel performance results have already been reported.[12,15,18-20]

VI. FUEL PERFORMANCE RESULTS AND ANALYSIS

VI.A. Prefailure Fuel Expansion

Fuel expansion measurements were based primarily on transient data from the hodoscope as well as on a comparison of data from hodoscope pre- and posttest static scans. Because fuel density can be very nonuniform near the fuel top, there is uncertainty of ~1% in the peak expansions given in Table IV, a significant quantity when the expansion is small. Concentrating on preirradiated test fuel, there is no indication of any shrinkage, and measured expansions tend to be significant in excess of ~1% that might be attributed to a purely thermal expansion. Good agreement between transient and posttest scan data implies that peak expansions persisted during cooldown. Expansions beyond pretest lengths are also evident in the posttest radiographs of intact pins shown in Fig. 11. The behavior of the single fresh pin tested ran counter to several of these trends and is discussed later.

It is also important to verify that the measured expansions extend over a significant portion of the fuel and are not simply an end effect of localized phenomena taking place near the fuel top. Basically, posttest density distribution measurements from all intact pins indicate fuel density reductions over the top half of the fuel, reflecting roughly the entire axial range where fuel melted during the transient. Examples are shown in

TABLE IV

Peak Overpower Conditions and Fuel Performance Summary

Fuel/ Cladding	Axial Peak Burnup (at.%)	Peak Overpower (Normalized[a])	Calculated Failure Threshold (Normalized[a])	Peak Pressure (MPa)	Maximum Axial Expansion (%)
U-19 Pu-10 Zr/ D9 steel	0.8[b]	4.3 (3.4)	5.1 (4.6)	1 (1)	1 (1)
	1.9[b]	4.3 (3.4)	5.1 (4.6)	3 (3)	2 (0.5)
	1.9	4.4	4.6	3	2 to 3
	5.3	4.4[c]	4.5	10	3
	9.8	4.0[c]	4.4	19	3
U-10 Zr/HT9 steel	2.9	4.8	4.4	6	2 to 4
U-5 Fs/Type 316 stainless steel	Fresh	3.8	4.3	0.6	4[d]
	0.3	4.1	4.7	0.6 to 0.8	16
	0.3	4.1	4.8	0.6 to 0.8	18
	2.4	4.1[c]	4.4	2 to 6	7
	4.4	4.2[c]	4.5	7 to 9	[e]
	4.4	4.0	4.4	7 to 9	4
	4.4	3.8	4.3	7 to 9	4
	7.9	4.1[c]	3.6 to 4.0	17 to 20	3
	7.9	3.4	3.6 to 4.0	17 to 23	4

[a]Relative to nominal conditions in a fast reactor: peak linear power of 40 kW/m, 630 K inlet, and 150 K coolant temperature rise.
[b]Indicates M5 test pins; values in parentheses are from the first overpower transient.
[c]Indicates cladding failure occurred.
[d]Expansion may have been caused by localized sodium bond boiling (see Sec. VI).
[e]Data ambiguous.

Fig. 12 from low-burnup U-Fs fuel that expanded by a total of 16 to 18%.

In comparing data from different fuel types, maximum prefailure expansion of the U-Fs test fuel shows large expansions at low burnup that decrease rapidly with increasing burnup. By contrast, prefailure axial expansion of IFR-type fuel showed much weaker burnup dependence with large values at low burnup conspicuously absent.

In irradiated fuel, the mechanism underlying measured axial expansion is believed to be fission gas that is initially confined within solid fuel, but freed to expand when fuel melts. Posttest examination of test pins that remained intact all show large bubbles. These are not typical of normal as-irradiated fuel but are indicative of extensive fuel melting, bubble coalescence, and expansion at much higher temperatures. A striking example of this behavior is shown in Fig. 13, which shows a vertical section from one of the low-burnup U-Fs pin described in Fig. 12. By contrast, in IFR-type fuel that expanded axially by only a few percent, fewer bubbles are found than in Fig. 13, but still more than in an untested sibling. Figure 14 shows a radial section of a ternary fuel pin that did not fail. Large bubbles are found at all axial locations where fuel had melted. Contrast should be made with untested ternary fuel shown in Fig. 1.

Postulating expanding fission gas as the driving mechanism, the following elements are needed to quantify the particular amount of axial expansion:

1. the amount of molten fuel
2. the concentration of gas made available to expand when fuel melts
3. initial size of gas bubbles (initial surface tension effects?)
4. the magnitude of the pin plenum pressure resisting expansion.

Axial expansion occurs when fission gas present in molten fuel expands until its pressure equals that of the pin plenum. The onset of fuel expansion coincides with significant fuel melting. Due to surface tension effects in the solid state, the initial volume occupied by fission gas depends on the initial bubble size. Small bubbles in the solid state indicate that gas is initially dissolved or packed within a very small volume and held by surface tension. If bubbles in the solid state are initially large, surface tension plays no role and fission gas is in equilibrium with plenum pressure.

During transient fuel heatup, individual bubbles expand in an attempt to maintain equilibrium of the internal pressure with the pin plenum pressure and the

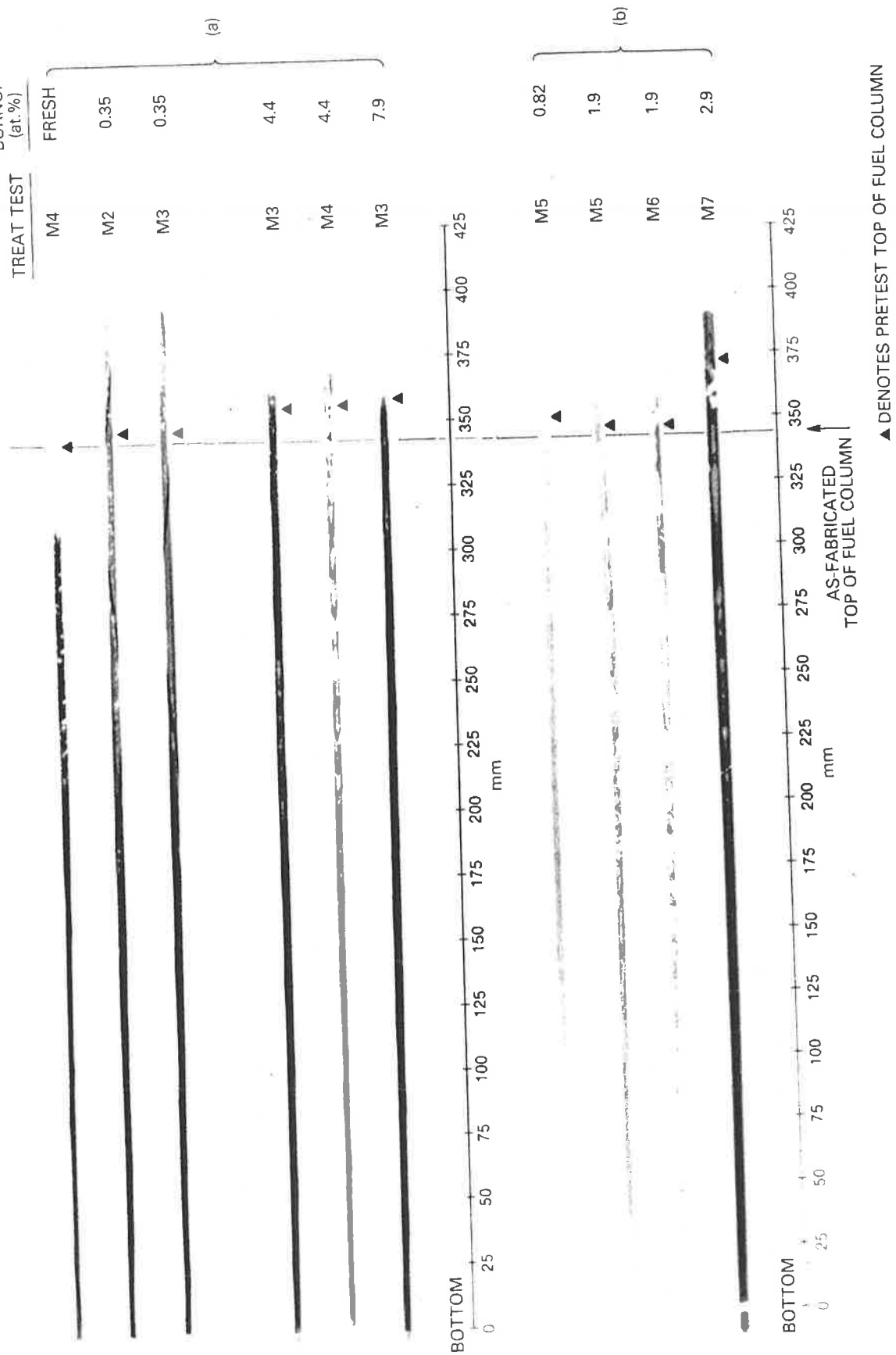

Fig. 11. Posttest radiographs of all M-series test pins that remained intact, illustrating permanent changes in length: (a) U-Fs and (b) IFR-type.

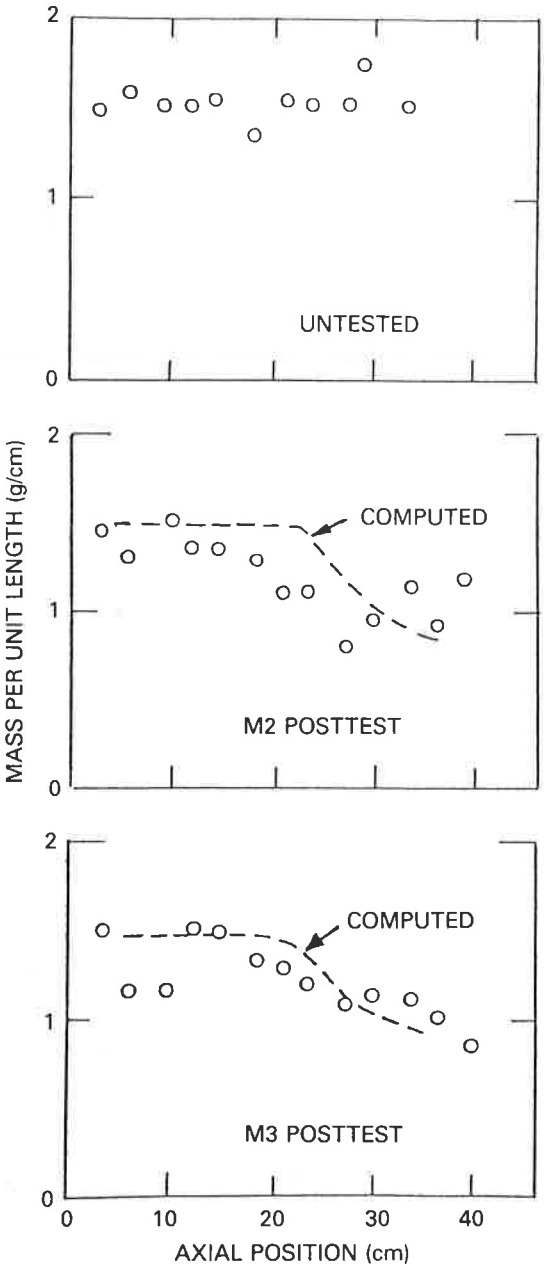

Fig. 12. Measured and computed posttest fuel mass distribution in low-burnup U-Fs fuel tested in M2 and M3.

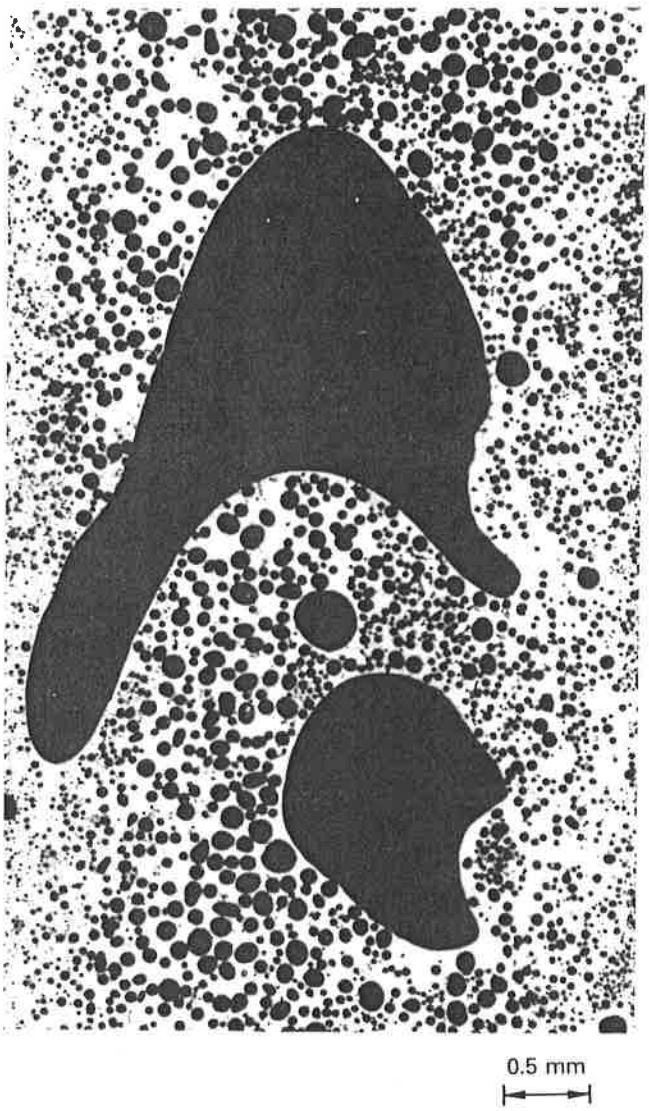

Fig. 13. Vertical section taken near the top of the M2 test pin described in Fig. 12.

bubble surface tension. While fuel is solid, bubble expansion rates are severely limited by various diffusion and creep processes.[5,21] Bubble coalescence is also extremely slow. At heating rates typical of M-series, expansion of solid fuel is computed to be negligibly small. However, once fuel melts, both expansion and coalescence are assumed to be sufficiently rapid that available fission gas expands instantly to equilibrium, regardless of initial bubble size (without any effect of surface tension). Thus, net expansion includes the effects of both bubble thermal expansion and, in the case of initially small bubbles, elimination of surface tension. Initially small bubbles would lead to greater net expansion upon melting than would large bubbles.

On cooldown, at least part of the expansion in an intact pin tends to be permanent. Because bubble coalescence is irreversible, all expansion due to coalescence is permanent. Also, expansion of individual bubbles can be permanent since little contraction occurs in the solid state after refreezing. However, large bubbles can rise and eventually escape to the pin plenum if cooldown is not quick enough. The shapes of the largest bubbles in Fig. 13 show some such evidence of rising.

Time-dependent computations of axial expansion in the tests were executed in the COBRA/EXP code

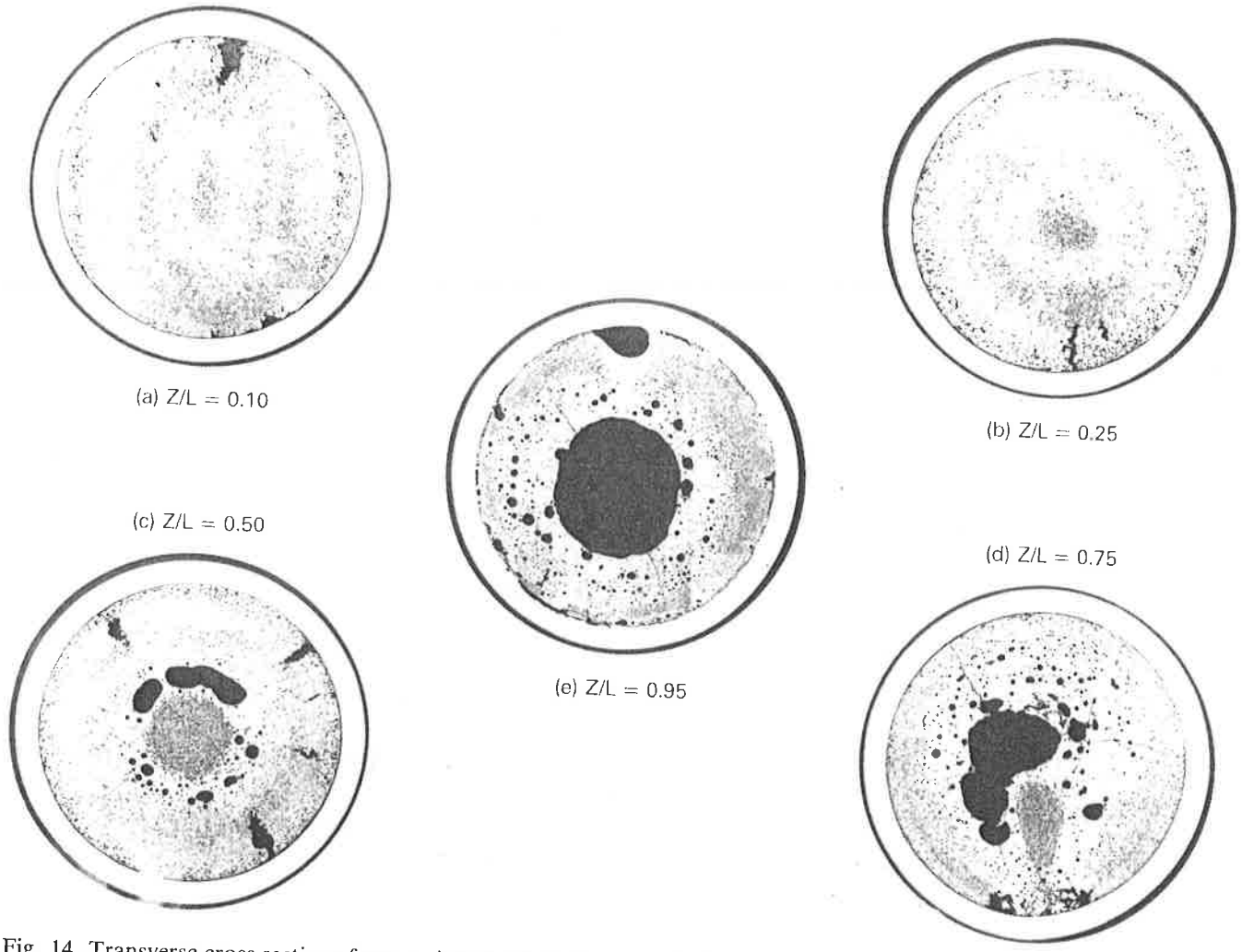

Fig. 14. Transverse cross sections from an intact 1.9 at.% burnup U-Pu-Zr pin tested in M5. Note extensive fuel melting at the highest three elevations and some melting attack on the cladding at the highest two elevations. Indicated elevations are relative to the as-fabricated fuel column.

module (see Sec. IV.D) using the thermal analyses described in Secs. IV and V. Thermal calculations estimated the amount of molten fuel at each axial node. Estimates of transient pin plenum gas pressure were based on sibling pin measurements at room temperature (Table II) and simply scaled upward in accord with the calculated absolute temperature of the pin plenum. (Peak values are given in Table IV.) A concentration of fission gas at each axial node and a typical bubble size were explicitly input to the computation. Computed expansion was averaged over the radial cross section of each axial node. Bubble rising was not included in the computation.

The same basic modeling was used to calculate axial expansions in all M-series tests but with significantly different concentrations of available fission gas assumed for U-Fs and IFR fuel types. Interestingly, if the measured expansions (Table IV) are calculated with this model, the amount of fission gas available for producing axial expansion is always much less than the amount of fission gas retained in the pin as a whole (Table II). This may be explained by the fact that local concentrations of dissolved gas decrease rapidly with irradiation temperature,[5] and it is basically the fuel with the least dissolved gas that melts first and contributes most to axial expansion.

The measured axial expansions in U-Fs fuel were large (15 to 20%) at low burnup but decreased rapidly as burnup increased. These expansions in U-Fs fuel were well predicted in timing, overall magnitude, axial distribution, and burnup dependence with the assumption of a maximum fission gas concentration in small bubbles of 5 μmol/g fuel (or the total gas generated in ~0.5 at.% of burnup). This assumed peak concentration, equal to about one-fourth of the peak whole-pin average amount, corresponded closely to measured gas concentrations at the hottest axial locations. Figure 15 shows the time dependence of the

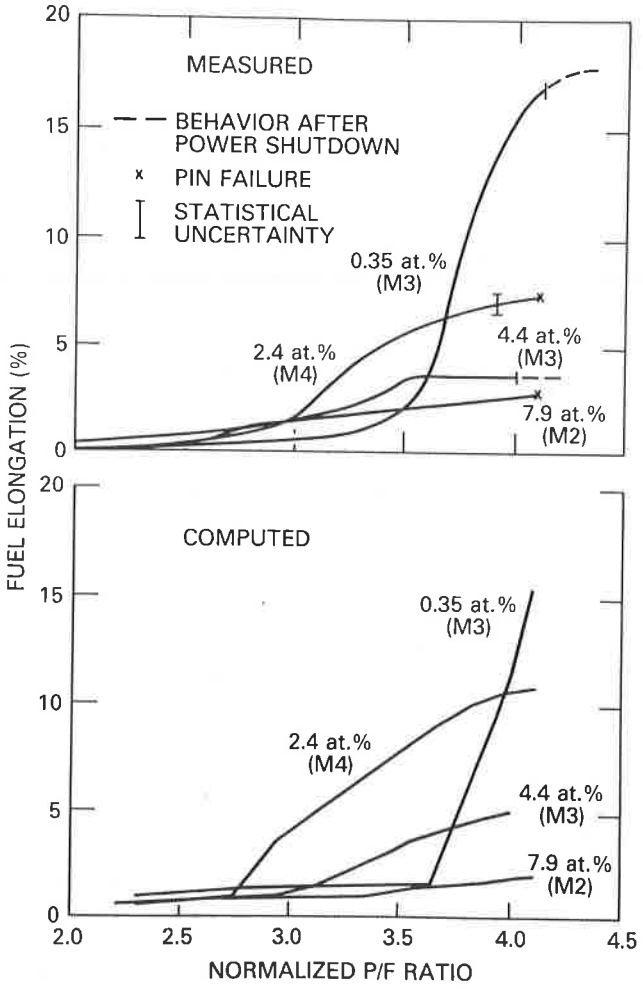

Fig. 15. Measured and computed time dependence of prefailure axial expansions: U-Fs fuel covering the range of tested burnup.

measured and computed axial expansion of selected U-Fs fuel pins, spanning the range of tested burnups. Timing on Fig. 15 is provided by the instantaneous overpower level. Permanence of the expansion upon cooldown was also predicted by the computation, as illustrated by the calculation shown compared to the measurement in Fig. 12.

By contrast, IFR fuel test data required rather different assumptions about fission gas availability. Assuming the same concentration of fission gas as employed successfully in the analysis of U-Fs fuel leads to predictions of expansion magnitudes that are too large and a burnup dependence that is too strong (similar to U-Fs fuel). Note, however, that the IFR fuel had a smaller grain size and was irradiated at a significantly higher linear power and temperature than the U-Fs fuel (Table II). Thus, the high-temperature regions of IFR fuel, which contribute most to axial expansion, might contain little, if any, dissolved gas. Expansions in IFR fuel were instead calculated assuming a model where only gas trapped in large bubbles within the fuel porosity was available for expansion. Because this gas is initially in equilibrium with the pin plenum pressure, the density of gas present in the pin's porosity is itself proportional to the plenum pressure. Expansion then depends principally on the temperature difference between molten fuel and the pin gas plenum. Axial expansions computed with this simple model of fission gas concentration do indicate approximately the right magnitude and the weak dependence on burnup that is present in the data reported in Table IV.

The behavior of the single fresh U-Fs pin provided an interesting counterpoint to that of irradiated fuel. Without benefit of any dissolved fission gas, there was evidence of ~4% local expansion near the top of the fuel peak power (Table IV), which collapsed rapidly on power shutdown (Fig. 11). Posttest examination showed evidence of large bubbles in the top region of the fuel. Local boiling of bond sodium entrained within molten fuel is a possible driving mechanism for this observed expansion. Computed fuel centerline temperatures near the fuel top were hot enough to vaporize sodium, and only a trace amount of liquid sodium in this region could have furnished the necessary vapor volume. Rapid collapse on cooldown is also consistent with condensible vapor being the expansion mechanism. Some residual bubbles, as were observed, could survive cooldown if the high-conductivity fuel were frozen faster than the vapor could condense.

VI.B. Cladding Failure Threshold

Two principal mechanisms have been identified[5,22] as causing cladding damage in metal fuel: overpressure and clad thinning. Due to the low mechanical strength of metal fuel, pin plenum pressure supplies the primary source of pressure loading and stress on the cladding. Cladding stresses, however, reflect not only the pin plenum pressure but also thinning by formation of a low-temperature uranium-iron eutectic.

Physical evidence exists from posttest remains to support and illustrate the two proposed mechanisms of cladding failure in metal fuel. Cross sections from an IFR pin that remained intact, shown in Fig. 14, illustrate an azimuthally nonuniform eutectic attack on the cladding in addition to the large bubbles of expanded fission gas mentioned previously. Figures 16a and 16b show sections of two M-series failure sites. Both failure sites were located at the top of the fuel. In Fig. 16a, the failure site of a medium-burnup (5.3 at.%) ternary pin shows strong evidence of cladding dissolution from the inside. (The attack evident on one outside surface was caused after failure by molten fuel ejected from the pin.) By contrast, the failure site of a higher burnup (7.9 at.%) U-Fs pin in Fig. 16b indicates cladding ballooning from pressure loading, with little indication of cladding dissolution from the inside. Both

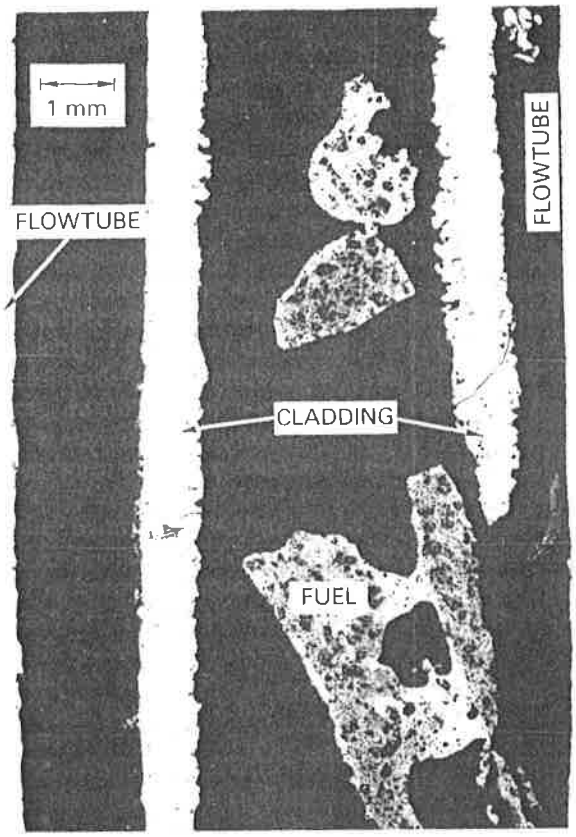

EUTECTIC PENETRATION (FROM M6)
(a)

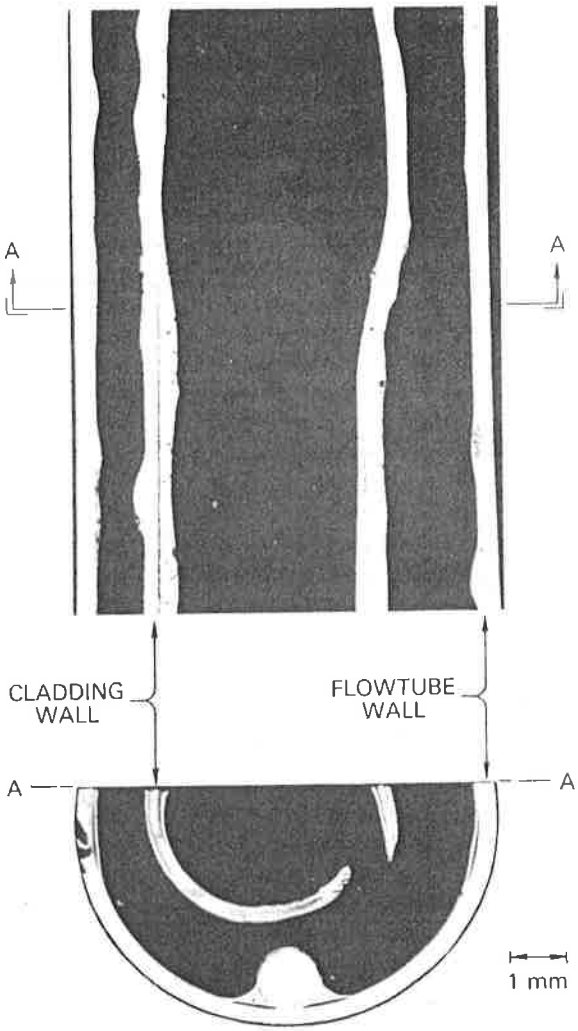

CREEP RUPTURE FROM PRESSURE LOADING IN A HIGH-BURNUP PIN (FROM M2)
(b)

Fig. 16. Representative pin failure sites at the top of the fuel: (a) 5.3 at.% burnup U-Pu-Zr pin (M6) and (b) 7.9 at.% burnup U-Fs pin (M2).

mechanisms appear in a third example of a failure site shown in Fig. 19.

Integrating these two damage mechanisms within a single analytical model to compute pin failure in metal fuel has been described[22] under the assumption that both mechanisms act independently. Cladding stress is first computed on the basis of computed gas plenum pressure and the remaining thickness of unreacted, load-bearing cladding. The calculation of transient pin plenum gas pressure is described in Sec. VI.A. (Peak values for M-series are given in Table IV.) Cladding damage by low-temperature melts seems closely related to alloys formed in a uranium-iron system. Above a threshold for the onset of eutectic formation (~1000 K), the rate of cladding penetration is strongly temperature dependent but shows little dependence on particular fuel or cladding type. In the model, cladding thickness is assumed to be reduced at a temperature-dependent rate correlated from laboratory measurements of iron dipped into melts of high uranium content, shown in Fig. 17. In the transient analysis, the computed temperature at the fuel/cladding interface is assumed to control cladding melt rate. A plastic strain rate is calculated from the computed cladding stress and temperature history using correlations derived from transient tube burst tests. Cladding failure is inferred when computed plastic strain exceeds a preset amount (2% for Type 316 stainless steel and D9 steel, and 6% for HT9 alloy). Detailed model calculations have been performed with the COBRA/EXP code

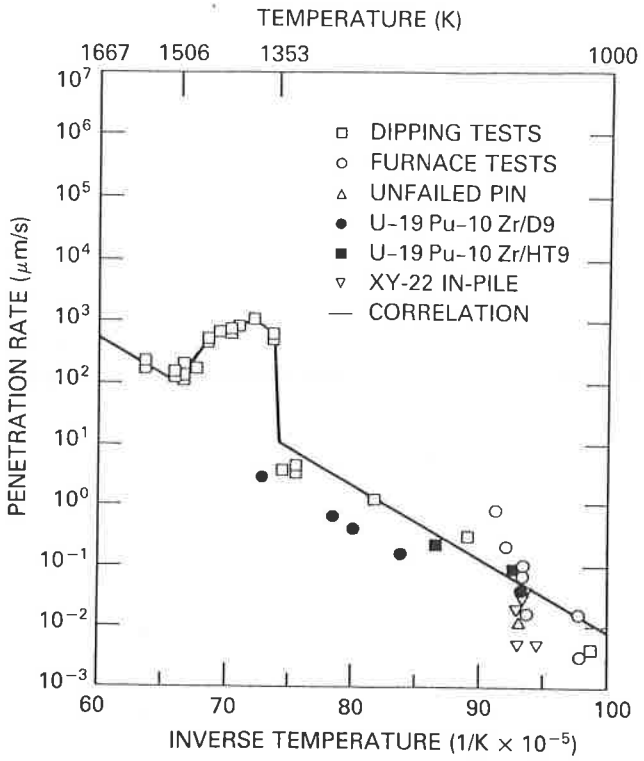

Fig. 17. Rates of cladding penetration by uranium-based melts as compiled from various sources.[22] The correlation shown is a fit to laboratory measurements of iron dipped into melts and supported by data from a wide range of actual fuel pins.

module (see Sec. IV.C) by linking this modeling scheme to the thermal analysis. A similar formulation of this model has also been incorporated in the FPIN2 code.[5]

These concepts may easily be applied to the present overpower test series in a semiquantitative fashion. The high thermal conductivity of metal fuel ensures peak cladding temperatures, hence likely failure sites, at the fuel top in agreement with observations. Temperatures, key to the failure threshold analysis (pin plenum, peak cladding midwall, and fuel/cladding interface temperatures), are close to or easily derived from the measured whole-pin coolant temperature rise. In conjunction with cladding failure observations, thermal calculations indicate that at overpower levels of ~4 times nominal, the temperature of the fuel cladding interface exceeds a threshold value of 1350 K, where Fig. 17 indicates eutectic penetration into the cladding becomes very rapid (associated with the melting of a protective solid iron-uranium compound).

Calculated times of cladding failure are also reported in Table IV, expressed in terms of overpower level on the actual ~8-s period power transient (or, if necessary an extension thereof). While these calculations are in no way definitive, observed cladding failures were in reasonable agreement with expectations, and with the noticeable exception of the U-Zr pin tested, no failures were expected in the pins that actually remained intact. While agreement between measured and calculated pin failures has always been reasonable (~5%), earlier tests (M2, M3, and M4), showed some systematic tendency for observed failures to precede the calculated ones. The possibility of hot spots locally generated around the cladding due to imperfect pin support is one physical mechanism that could induce failures earlier than anticipated, and improvements in pin mounting methods described in Sec. III.C may have helped alleviate this potential problem. The survival of the U-Zr pin, tested to ~4.8 times nominal power, was quite unexpected, not only because calculated failures have tended to lag behind observed cladding failures, but also because computed temperatures far exceeded the expected threshold for rapid eutectic penetration.

Figure 18 shows a cross section of the surviving U-Zr pin at the top of the fuel. While there is evidence for a great deal of molten fuel in the central regions of this cross section, the cladding was in contact with only a thin region of molten fuel. The cladding penetration shown is azimuthally irregular and extends to a maximum depth of ~30% of its original thickness. Based on the computed thermal history of the pin, this observed amount of penetration, while large, is a factor of ~10 less than expected from the correlation of Fig. 17.

The key to understanding the unexpected survival of the U-Zr pin may be the observation that a significant amount of fuel near the cladding never melted. Proper application of the Fig. 17 melt rate correlation requires a molten phase, rich in uranium, in contact with the cladding. For this to happen, melting at the interface must involve a much higher proportion of fuel volume than cladding volume (by a factor of ~5 to 15), but in Fig. 18 the volumes of fuel and cladding involved in the melt near the interface are approximately equal. Thus, any delay in melting of fuel inward from the cladding would be expected to also slow the penetration into the cladding. In the U-Zr pin, such a delay might have been caused by the binary fuel's high solidus temperature of 1500 K. In contrast, in all the other metal fuels tested thus far, lower solidus values ensured an entirely molten fuel cross section when the threshold for rapid melt penetration (~1350 K) was reached at the fuel/cladding interface.

General analytical studies with the cladding failure model[5,22] indicate that the cladding damage induced in M-series tests so far was strongly weighted to high cladding temperatures of ~1350 K. Typically, at M-series heating rates, nearly total eutectic penetration would be required to fail cladding at low burnup, partial penetration would be required at midrange burnups, and almost no penetration would be required at high burnup. The abrupt rise of eutectic penetration

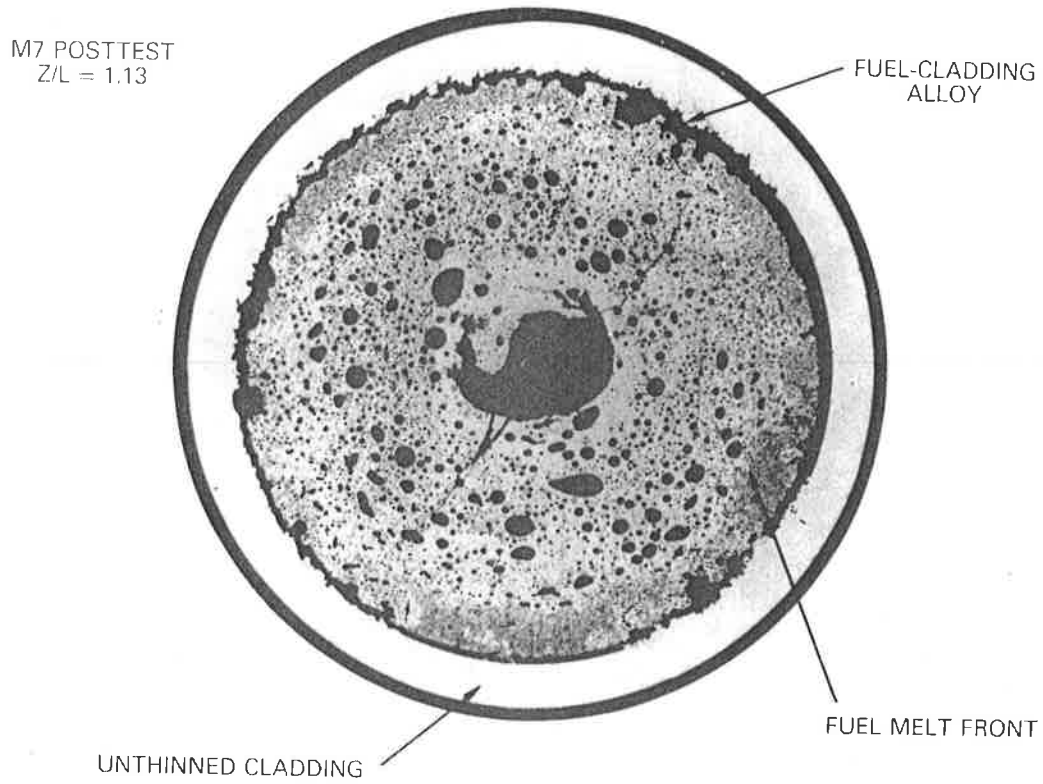

Fig. 18. Cross section at the top of the damaged but intact U-Zr pin tested in M7, illustrating once-molten fuel, once-molten fuel/cladding alloys, and extensive cladding damage. The indicated elevation is relative to the as-fabricated fuel column.

rate at overpower levels ~4 times nominal was a dominating factor, and only calculations for the highest burnup pins suggest a controlling role for pressure loading (although still at high temperature). In these tests, margin to failure was not expected to depend strongly on the particular cladding type. At low temperatures, mechanical calculations do formally distinguish between properties of different cladding types (in both strain rates and plastic strain to failure), but since most strain occurred at high temperatures the computed differences were negligible. Future tests either with higher burnup fuel or with more slowly rising overpower transients could induce cladding damage at lower temperatures and highlight differences in cladding type.

VI.C. Postfailure Events

When cladding failed, similar postfailure events characterized the behavior of all fuel types tested. In each case, about half of the fuel inventory, corresponding roughly to the fuel melt fraction, was ejected rapidly through a small cladding breach at the fuel top. Cladding failure was always accompanied by a sudden, temporary reversal of inlet coolant flow and rapid coolant voiding. Measured pressure spikes were minor (<2 MPa) and were generally about one order of magnitude less than the plenum pressure of the failed pin. Fuel ejection from a failed pin could be driven by expansion of trapped fission gas or sudden boiling of the liquid sodium bond within the fuel. Ejected fuel then dispersed rapidly, combining with cladding and structural materials into a highly mobile low melting point eutectic and traveling upward with the coolant to locations well downstream of the original fuel zone. Hodoscope data indicate the time of significant disruption and removal to be ~100 to 200 ms. This timing is also in agreement with measured perturbations of pressure and flow. Afterward, coolant flow past failed pins settled at ~$\frac{2}{3}$ of its prefailure value, indicating only partial flow blockage.

Figure 19 shows cross sections at various axial locations of a failed 9.8 at.% burnup ternary pin, indicating fuel losses and remains of primarily solid but disrupted fuel. (Figure 19 also depicts the failure site, showing evidence of cladding ballooning under pressure and melting attack.) Interestingly, in studying the remains of all M-series failed pins, the amount of in-pin disruption of solid fuel after failure depends on both burnup and fuel type. For a given fuel type, the

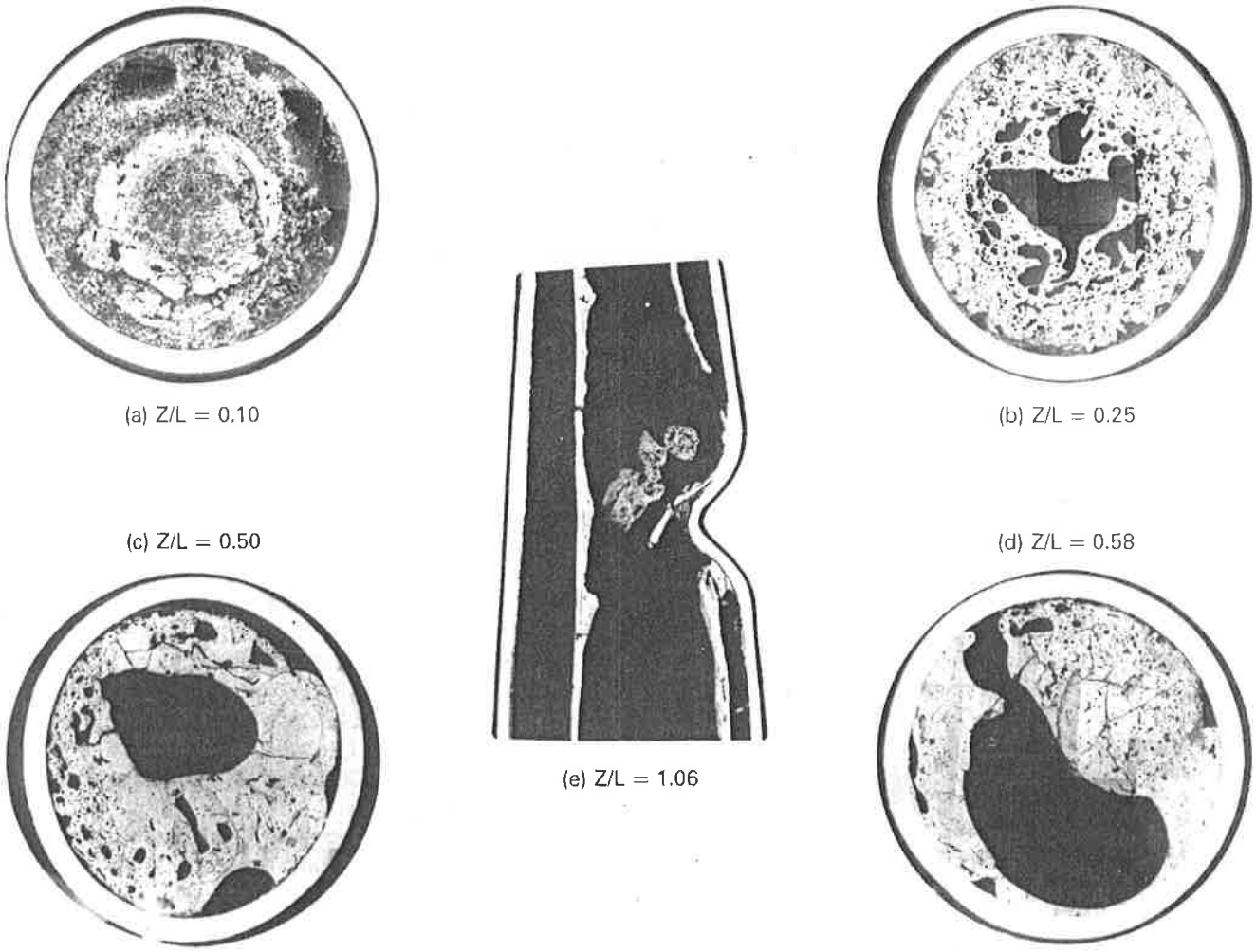

Fig. 19. Transverse cross sections and failure site from a failed 9.8 at.% burnup U-Pu-Zr pin tested in M7. The failure site shows damaged cladding and a bent flowtube. Little fuel was found above the highest transverse cross-section elevation shown. The indicated elevations are relative to the as-fabricated fuel column.

amount of in-pin disruption of primarily solid fuel showed strong increases with burnup or, equivalently, the amount of pin depressurization following failure. However, much more of the solid fuel remains stayed in place in failed IFR fuel than in tests with U-Fs fuel. Since IFR fuel contained significantly less dissolved gas than U-Fs fuel, the difference suggests a gas-driven disruption mode for solid fuel. The neutron radiographs of all failed M-series pins shown in Fig. 20 illustrate these features. Besides extensive fuel losses, attention is also directed to the varying amounts of apparently intact fuel remaining in the lower portion of each pin. In contrast, the amount of unmelted fuel computed at peak power was very similar for each test pin.

After reactor power shutdown in tests where pins failed, gamma rays characteristic of isotopes ^{89}Rb, ^{138}Cs, and ^{138}Xe were detected in the gas space above the loop plenum by the developmental FPDS. None were detected from tests in which all pins remained intact. These observations are at present qualitative, but the observed isotopes likely originated from the following chain of fission product release and transport:

1. Fission products ^{89}Br and ^{138}I, which are soluble in sodium, were released from the fuel and transported efficiently in the coolant.

2. Bromine-89 and ^{138}I decayed into noble gases, ^{89}Kr and ^{138}Xe, which escaped into the gas plenum.

3. Krypton-89 and ^{138}Xe decayed into ^{89}Rb and ^{138}Cs, which settled out on the loop wall.

VII. CONCLUSIONS

Methods and techniques have been developed for multiple-pin overpower test-to-failure of various types

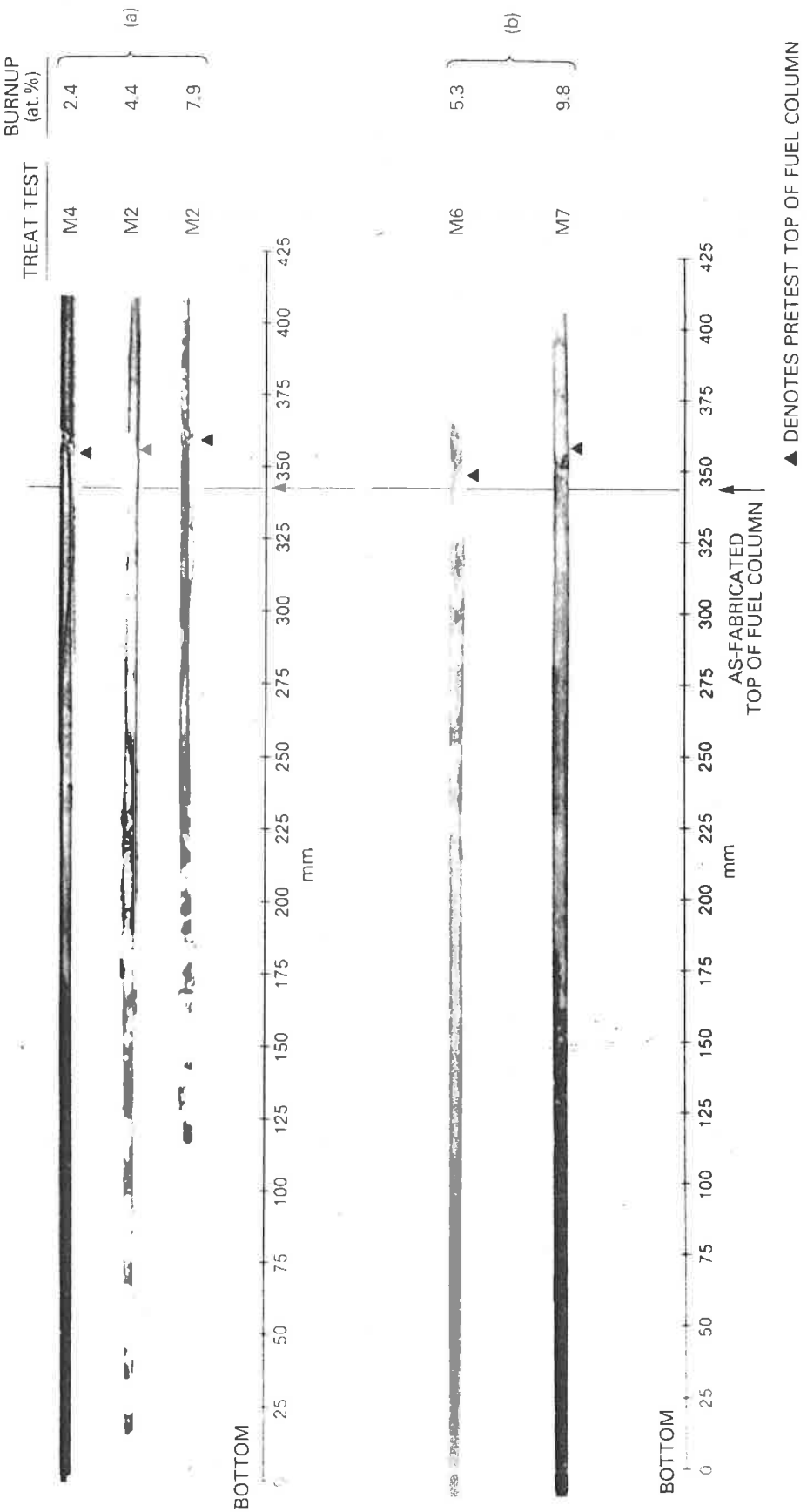

Fig. 20. Posttest radiographs of all M-series test pins that failed, illustrating both extensive fuel removal and differing amounts of fuel remaining intact: (a) U-Fs and (b) IFR-type.

of modern metallic fuel. During the program, hardware improvements in test pin mounting and instrumentation led to improved knowledge and control of each test pin's power and coolant flow rate during the overpower transient. Relatively simple adjustments or enhancements of test conditions also improved the simulation of prototypical fast reactor fuel temperatures. Peak overpower conditions calculated in the test fuel were confirmed by comparison of measured and calculated temperature rises. Posttest measurements of maximum melting extent in intact test pins also helped to confirm calculated peak amounts of fuel melting needed for subsequent analysis.

Simple models of prefailure expansion and cladding failure were developed and validated. While the safety-related fuel behavior of all fuel types tested was similar, the fuel properties of fission gas retention and melting point were found to account for observed differences. The prefailure axial expansion in irradiated fuel was always positive and significant beyond thermal expansion. Large expansions at low burnups were measured in U-Fs fuel, but not measured in IFR-type fuel. At medium-to-high burnup, expansions in the range of 2 to 4% were typical of all fuel tested. Expansion of fission gas trapped in melting fuel provides a sound basis for modeling axial expansions, and differences in amounts of dissolved gas account for measured expansion differences between fuel types. The cladding failure threshold with the 8-s period overpower conditions is ~4 times nominal power over a wide range of burnups and fuel types tested. From the M-series data base generated thus far, successful cladding failure models should include effects of both overpressure and penetration of cladding by low-temperature melts. Because rapid cladding penetration by melts also requires extensive fuel melting, failure might be delayed somewhat in a fuel with a high melting point, such as U–10 Zr.

Studies with the present cladding failure model indicate that, for the fuel burnups and heating rates employed in M-series tests, pins fail at or near the threshold point of rapid eutectic penetration. Different modeling issues and questions arise concerning slower cladding damage rates at lower temperatures. Extending model validation into these areas requires testing higher burnup fuel and overheating test fuel to lower temperatures for longer times.

Postfailure disruption in all fuel types tested involved a benign ejection of the failed pin's inventory of molten fuel through a small local breach at the top of the fuel. Extensive disruption of the solid fuel remaining within failed pins is possible if a significant amount of fission gas is dissolved in that fuel. Once ejected, molten fuel was highly mobile in the coolant channel, showing little tendency to cause blockages. There is strong evidence from posttest remains that molten and mobile fuel in the coolant channel is in a low melting point eutectic form. Because the coolant channel environment in the tests was not optimized to simulate a large pin bundle, only qualitative conclusions should be drawn concerning dispersal of materials from failed pins.

ACKNOWLEDGMENTS

Performance of an experimental program of this magnitude requires the professional efforts of many more individuals than the five authors. Accordingly, we would like to acknowledge significant contributions from the ANL staff at both the Illinois and Idaho sites, including the following persons: T. T. Anderson, C. August, A. M. Barczak, N. J. Carson, H. W. Helenberg, E. W. Johanson, D. A. Kraft, H. J. Myers, R. A. Noland, and R. J. Robertson for experiment design and operations; T. H. Braid, A. DeVolpi, C. E. Dickerman, J. P. Regis, and G. S. Stanford for nuclear diagnostics; J. F. Kerr, W. Kettman, H. V. Rhude, K. T. Teraguchi, and G. M. Teske for handling disassembly and posttest examination; L. J. Harrison, N. A. Kramer, G. R. Larsen, D. M. Ray, and W. W. Stevens for TREAT operations; R. D. Baldwin, D. J. Dever, P. H. Froehle, M. R. Kraimer, G. R. Klotzkin, R. K. Lo, R. W. Swanson, and R. Villarreal for analysis support; and A. J. Goldman, J. E. Herceg, A. E. Klickman, J. M. Kramer, and R. H. Sevy for general guidance, management, and advice.

This work was supported by the U.S. Department of Energy under contract W-31-109-Eng-38.

REFERENCES

1. J. E. CAHALAN, J. M. KRAMER, J. F. MARCHATERRE, C. J. MUELLER, D. R. PEDERSEN, R. H. SEVY, D. C. WADE, and T. Y. C. WEI, "Integral Fast Reactor Safety Feature," *Proc. Int. Topl. Mtg. Safety of Next Generation Power Reactors*, Seattle, Washington, May 1–5, 1988, p. 103, American Nuclear Society (1988).

2. L. C. WALTERS, B. R. SEIDEL, and J. H. KITTEL, "Performance of Metallic Fuel and Blankets in Liquid-Metal Fast Breeder Reactors," *Nucl. Technol.*, **65**, 179 (1984).

3. R. E. EINZIGER and B. R. SEIDEL, "Irradiation Performance of Metallic Driver Fuel in Experimental Breeder Reactor II to High Burnup," *Nucl. Technol.*, **50**, 25 (1980).

4. R. G. PAHL, C. E. LAHM, and R. VILLARREAL, "Recent Irradiation Tests of Uranium-Plutonium-Zirconium Metal Fuel Elements," *Proc. Int. Conf. Reliable Fuels for Liquid Metal Reactors*, Tucson, Arizona, September 7–11, 1986, p. 3, American Nuclear Society (1986).

5. J. M. KRAMER, T. H. HUGHES, and E. E. GRUBER, "Validation of Models for the Analysis of the Transient Behavior of Metallic Fast Reactor Fuel," *Proc. 10th Int. Conf. Structural Mechanics in Reactor Technology*, Anaheim, California, August 14–18, 1989, p. C-65, International Atomic Energy Agency (1989).

6. R. A. diNOVI, "Effect of Burnup and Irradiation on Thermal Diffusivity and Conductivity of Uranium-Fission Alloy," ANL-7889, Argonne National Laboratory (Jan. 1972).

7. W. N. BECK and R. J. FOUSEK, "In-Pile Measurement of Fission Gas Release and Change in Thermal Conductivity for U–5 wt.% Fs Alloy," *Trans. Am. Nucl. Soc.*, **23**, 1 (1969).

8. P. R. BETTEN, "In-Core Measurements of Uranium–5 wt% Fissium Alloy Thermal Conductivity," *Trans. Am. Nucl. Soc.*, **51**, 239 (1985).

9. A. DeVOLPI, C. L. FINK, G. E. MARSH, E. A. RHODES, and G. S. STANFORD, "Fast-Neutron Hodoscope at TREAT: Methods for Quantitative Determination of Fuel Dispersal," *Nucl. Technol.*, **56**, 141 (1982).

10. A. E. WRIGHT, J. P. BURELBACH, N. J. CARSON, C. E. DICKERMAN, J. B. HEINEMAN, A. E. KLICKMAN, R. A. NOLAND, R. J. PAGE, L. E. ROBINSON, and J. P. TYLKA, "Mark-III Integral Sodium Loop for LMFBR Safety Experiments in TREAT," *Proc. Conf. Fast, Thermal, and Fusion Reactor Experiments*, Salt Lake City, Utah, April 12–15, 1982, p. I-174, International Atomic Energy Agency (1982).

11. A. E. WRIGHT, T. H. BAUER, W. R. ROBINSON, and A. E. KLICKMAN, "Techniques of Metal Fuel Transient Testing in TREAT," *Proc. Int. Topl. Mtg. Safety of Next Generation Power Reactors*, Seattle, Washington, May 1–5, 1988, p. 871, American Nuclear Society (1988).

12. T. H. BAUER, A. E. WRIGHT, W. R. ROBINSON, A. E. KLICKMAN, and J. W. HOLLAND, "Behavior of Metallic Fuel in TREAT Transient Overpower Tests," *Proc. Int. Topl. Mtg. Safety of Next Generation Power Reactors*, Seattle, Washington, May 1–5, 1988, p. 857, American Nuclear Society (1988).

13. P. H. FROEHLE and T. H. BAUER, "COBRA-PI: An Extension of the COBRA-3M Code Dynamically Dimensioned to Accept Pin Bundles of Any Size," *Proc. ANS Mathematics and Computation Division Topl. Mtg. Advances in Reactor Computations*, Salt Lake City, Utah, March 28–31, 1983, p. 211, American Nuclear Society (1983).

14. W. R. ROBINSON, R. K. LO, A. E. WRIGHT, T. H. BAUER, G. S. STANFORD, and J. A MORMAN, "Integral Fast Reactor Safety Tests M2 and M3 in TREAT," *Trans. Am. Nucl. Soc.*, **50**, 352 (1985).

15. T. H. BAUER, A. E. KLICKMAN, R. K. LO, E. A. RHODES, W. R. ROBINSON, G. S. STANFORD, and A. E. WRIGHT, "Behavior of Uranium-Fissium Fuel in TREAT Transient Overpower Tests," *Trans. Am. Nucl. Soc.*, **53**, 306 (1986).

16. W. R. ROBINSON, T. H. BAUER, A. E. WRIGHT, E. A. RHODES, G. S. STANFORD, and A. E. KLICKMAN, "First TREAT Transient Overpower Tests on U-Pu-Zr Fuel: M5 and M6," *Trans. Am. Nucl. Soc.*, **55**, 418 (1987).

17. W. R. ROBINSON, A. E. WRIGHT, T. H. BAUER, W. R. ROBINSON, D. A. KRAFT, and A. E. KLICKMAN, "IFR Overpower Test M7 in TREAT," *Trans. Am. Nucl. Soc.*, **56**, 383 (1988).

18. E. A. RHODES, G. S. STANFORD, and J. P. REGIS, "Motion of IFR Metal-Alloy Fuel in TREAT Experiment M7," *Trans. Am. Nucl. Soc.*, **56**, 384 (1988).

19. A. E. WRIGHT, T. H. BAUER, R. K. LO, W. R. ROBINSON, and R. G. PALM, "Recent Metal Fuel Safety Tests in TREAT," *Proc. Int. Conf. Science and Technology of Fast Reactor Safety*, Guernsey, England, May 12–16, 1986, Vol. 1, p. 59, American Nuclear Society (1986).

20. J. W. HOLLAND, A. E. WRIGHT, T. H. BAUER, A. J. GOLDMAN, A. E. KLICKMAN, and R. H. SEVY, "Posttest Examination Results of Recent TREAT Tests on Metal Fuel," *Proc. Int. Conf. Reliable Fuels for Liquid Metal Reactors*, Tucson, Arizona, September 7–11, 1986, American Nuclear Society (1986).

21. E. E. GRUBER and J. M. KRAMER, "Gas-Bubble Growth Mechanisms in the Analysis of Metal Fuel Swelling," *Proc. 13th Int. Symp. (Part I) Radiation-Induced Changes in Microstructure*, Phildelphia, 1987, ASTM-STP-955, p. 432, American Society for Testing and Materials (1987).

22. T. H. BAUER, G. R. FENSKE, and J. M. KRAMER, "Cladding Failure Margins for Metallic Fuel in the Integral Fast Reactor," *Proc. 9th Int. Conf. Structural Mechanics in Reactor Technology*, Lausanne, Switzerland, August 17–21, 1987, p. C-31, International Atomic Energy Agency (1987).